Saturation Point Analysis of Moist Convective Overturning

ALAN K. BETTS

West Pawlet, VT 05775

(Manuscript received 26 May 1981, in final form 25 January 1982)

ABSTRACT

A unified approach to the thermodynamics of cloudy air, cloud-clear air mixing processes, atmospheric thermodynamic equilibrium structure and instability is formulated, using a new concept: the *Saturation Point*. This permits the representation of mixing processes and virtual potential temperature isopleths for clear and cloudy air on a thermodynamic diagram (a tephigram is used here), and their comparison with the atmospheric stratification. Illustrative examples will be given for evaporative mixing instability and convective equilibrium structure for stratocumulus, cumulus and cumulonimbus convection and convection in the incipient severe storm atmosphere.

1. Introduction

This paper introduces a new unified approach to the thermodynamics of cloudy air (but not the formation of precipitation) and the relationship of the vertical structure of the convective atmosphere to cloud mixing processes and convective overturning. Illustrative examples will be taken from stratocumulus, cumulus, cumulonimbus and convection in the incipient severe storm atmosphere. Some of the concepts are new; others are a consolidation of previous research by many authors. A key new concept, the *Saturation Point* (SP; see Section 2) and a corresponding Saturation Level (SL) will be introduced to represent the properties of clear and cloudy air (but not precipitation particles). For unsaturated air, the SL is the familiar lifting condensation level (LCL). In general, however, we may use the Saturation Point concept to understand mixing processes between cloud and environment, and to interrelate updraft and downdraft structure, atmospheric stratification and stability. Extensive use will be made of the tephigram to illustrate these concepts. Other thermodynamic diagrams could easily be substituted. The use of the SP also permits the representation of virtual potential temperature for both clear and cloudy air on a tephigram which facilitates the visual understanding of cloud parcel buoyancy as well as atmospheric instability and equilibrium structure. These are significant advances in the use of the thermodynamic diagram.

This paper draws on many strands of research. Rossby (1932) introduced the equivalent potential temperature and discussed characteristic curves and mixing processes for air mass thermodynamic properties on an equivalent potential temperature diagram. The Saturation Point analysis of this paper can be regarded as a generalization of his work to include cloudy air. Betts (1973) discussed the modeling of the mixed layer and non-precipitating cumulus convection and introduced the liquid water potential temperature (θ_L), a conserved parameter for reversible moist processes, in addition to total water (q_T) and the equivalent potential temperature (θ_E). Betts (1978) summarized and extended these ideas using tephigram plots of convective parcel paths for conserved parameters. The Saturation Point concept carries this synthesis a stage further by representing conserved parcel properties by a single point on a thermodynamic diagram. This reduces cloud–environment mixing processes, for example, to mixing between two points. The papers on the modeling and stability of stratocumulus layers (Lilly, 1968; Schubert, 1976; Deardorff, 1976, 1980; and Randall, 1980) have influenced this approach. Deardorff (1980) in particular presented a diagrammatic representation of cloud-top entrainment instability for stratocumulus, using the conserved parameters and total water. Here, we shall reformulate this problem using the Saturation Point and a tephigram to draw parallels with the severe storm atmosphere and cumulus convection.

This paper was particularly influenced by Paluch (1979) who presented diagrams for cloud-top mixing into cumulus over land, and the formation of downdrafts. Here, we shall show that, using the Saturation Point, the tephigram (or other thermodynamic diagrams) can be used to represent this process in a highly compact manner and indeed to compare the properties (including buoyancy) of all mixtures of cloud and environment at any level. Telford (1975) has also discussed the thermodynamics of mixing processes between cloud and environment.

The formation of downdrafts, particularly in se-

0022-4928/82/071484-22$09.50

vere storms (e.g., Fujita and Caracena, 1977) is of considerable interest. Betts and Silva Dias (1979) presented a model for an unsaturated downdraft using an evaporation pressure scale, and noted the significance of the LCL for downdraft outflow air. Here we shall address unsaturated downdrafts driven by evaporation only briefly, although another process is considered: how downdrafts can be initiated in the incipient severe storm atmosphere by cloud–clear air mixing processes.

The equilibrium structure of the convective atmosphere will also be addressed. This has been influenced by the work of Ludlam (1966, 1980) as well as Betts (1973), Albrecht *et al.* (1979) and Arakawa and Schubert (1974).

The aim of this paper is to demonstrate the usefulness of the Saturation Point concept in understanding convective processes and convective overturning. Linear approximations will be used in many places for illustration, although these are not satisfactory for numerical computation.

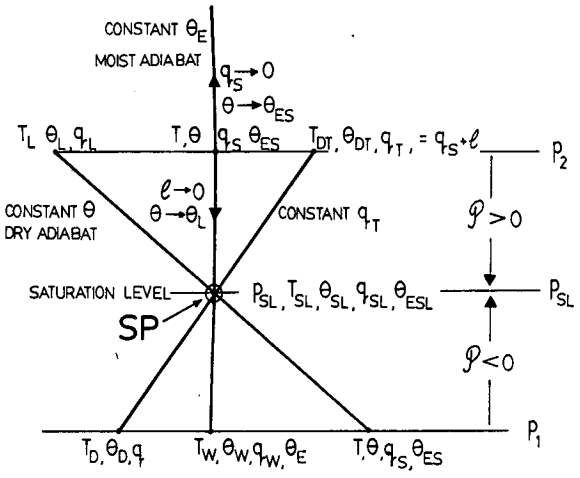

FIG. 1. Sketch thermodynamic diagram (tephigram), showing the relationship of Saturation Point SP (T_{SL}, p_{SL}) to the conserved parcel properties (θ_{SL}, θ_{ESL}, q_{SL}) which are independent of parcel pressure, and to the parcel properties at other pressure levels, such as (T, T_W, T_D) at p_1, for unsaturated air (for which $\mathcal{P} < 0$). The arrows on the moist adiabat denote the paths of integration of (2b) and (2c) in the definition of θ_{ES}, θ_L respectively.

2. Saturation point formulation of moist thermodynamics

a. Conservative variables with cloud water

In this paper, we distinguish between cloud water and precipitation water with a fall-speed significant compared with vertical air motions. Cloud water is treated as a parcel property. The difference between the pseudoadiabat and the reversible adiabat will be neglected (we shall simply refer to the moist adiabat), as will freezing processes. To this approximation, the variables q_T, θ_E, θ_L are conserved in adiabatic motions in non-precipitating cloud systems and are defined by integrating the three approximate equations (Betts, 1973)

$$0 = dq_T = dq_S + dl, \tag{1a}$$

$$0 = C_p \frac{d\theta_{ES}}{\theta_{ES}} = C_p \frac{d\theta}{\theta} + L \frac{dq_S}{T}, \tag{1b}$$

$$0 = C_p \frac{d\theta_L}{\theta_L} = C_p \frac{d\theta}{\theta} - L \frac{dl}{T}. \tag{1c}$$

The chief approximation is the use of dry air values for the specific heat and the gas constant (in the definition of θ). Clearly only two of these equations are independent. Integration gives

$$q_T = q_S + l, \tag{2a}$$

$$\ln\left(\frac{\theta_{ES}}{\theta}\right) = \int_0^{q_S} L dq_S / C_p T, \tag{2b}$$

$$\ln\left(\frac{\theta_L}{\theta}\right) = -\int_0^{l} L dl / C_p T. \tag{2c}$$

The integrals are both evaluated along the moist adiabat through a cloudy parcel (θ, q_S, p), but in opposite directions since θ_{ES} is that value of θ where $q_S = 0$, and θ_L that value of θ where $l = 0$ (see Fig. 1). Just as θ_E is the highest value of θ attainable by condensing all the vapor q_S, so θ_L is the lowest θ attainable by evaporating all the parcel cloud water. (An appropriate nomenclature would be condensation potential temperature for θ_E and evaporation potential temperature for θ_L, but the corresponding subscript change would be very confusing, so we shall retain the conventional names: equivalent potential temperature for θ_E and liquid water potential temperature for θ_L).

Because the latent heat L and parcel temperature T vary along the moist adiabat, the integrals in (2) must be evaluated numerically or using empirical functions (Simpson, 1978; Bolton, 1980 for θ_E) or approximated. For most observational purposes, it is sufficiently accurate (error ~0.2 K at warm temperatures) to approximate the integrals as (see Bolton, 1980, for θ_E)

$$\ln(\theta_{ES}/\theta) = 2.67 q_S / T, \tag{3a}$$

$$\ln(\theta_L/\theta) = -2.37 l / T, \tag{3b}$$

where (3b) is accurate for saturation pressure differences (see next section) ≤300 mb. These formulas are useful because they contain only parcel parameters at one pressure level. The coefficients differ because the integrations are in opposite directions along the moist adiabat (Fig. 1). For unsaturated air θ_E is given by

$$\ln(\theta_E/\theta) = 2.67 q / T_{SL}, \tag{3c}$$

where T_{SL} is the temperature at the LCL or saturation level, which can be readily computed from parcel parameters. θ_L for unsaturated air reduces to θ, and q_T to vapor mixing ratio q.

The conventional approximations of (2b), (2c) for θ_{ES}, θ_L are

$$\theta_{ES}/\theta \approx \exp(Lq_S/C_pT), \tag{4a}$$

$$\theta_L/\theta \approx \exp(-Ll/C_pT) \approx 1 - (Ll/C_pT). \tag{4b}$$

Because $q_S > l$, typically, (4a) is a somewhat worse approximation than (4b), and the corresponding first-order expansion of (4a) is even worse and rarely used. [Inverting (4a) and expanding

$$\theta/\theta_{ES} \approx \exp(-Lq_S/C_pT) \approx 1 - (Lq_S/C_pT) \tag{4a'}$$

gives a somewhat better approximation, but (3a) is more accurate.]

Consider the reversible adiabatic ascent of an air parcel from p_1 through its LCL to p_2 (Fig. 1). On this thermodynamic diagram, the familiar paths of temperature (T), wet-bulb temperature (T_W) and dewpoint (T_D) (corresponding to constant θ, θ_E, q) converge to a point at the lifting condensation level (LCL) which is here called the saturation level (SL). As the parcel passes its SL and becomes cloudy the three paths diverge, and now correspond to constant θ_L, θ_{ES}, q_T (Betts, 1973, 1978). The paths of θ_L, q_T depend on cloud water content [see (2a), (2c)] as well as (T, p), while θ_{ES} is a function of parcel (T, p) only.

b. *The saturation point*

The three lines in Fig. 1 representing the conservation of three variables [(θ, θ_E, q) for unsaturated air and (θ_L, θ_{ES}, q_T) for cloudy air] intersect at a point, where the temperature and pressure (T_{SL}, p_{SL}) completely specify the three conserved parameters, which we shall represent by θ_{SL}, θ_{ESL} and q_{SL}. We shall call this point the *Saturation Point* (SP) and the pressure level at which it occurs the *Saturation Level* (SL). Viewed from below (the unsaturated side) this level has long been called the Lifting Condensation Level (LCL); viewed from above it has been called the Sinking Evaporation Level (SEL) by Betts (1978). The more general terminology is of value, since (T_{SL}, p_{SL}) and the three derived conserved parameters do not change with the reference level of an observation. In this frame of reference, the thermodynamic state of an air parcel is specified by the Saturation Point properties (T_{SL}, p_{SL}) and its pressure difference from the Saturation Level, i.e.,

$$\mathcal{P} = p_{SL} - p. \tag{5}$$

On a thermodynamic diagram, air parcels that have a given (T, p) may have SL's at any level, p_{SL}, depending on their total moisture content. Parcels with total moisture content $q_T > q_S(T, p)$ will be saturated and cloudy with $\mathcal{P} > 0$, while if parcel $q < q_S(T, p)$, it will be unsaturated with $\mathcal{P} < 0$ [this sign convention is the reverse of Betts and Silva Dias (1979)]. Positive $\mathcal{P}$ is directly related to liquid water content [Eq. (A5')]; negative $\mathcal{P}$ to subsaturation. Only if $l = 0$, and the parcel is just saturated, does $p = p_{SL}$, $\mathcal{P} = 0$.

We shall call $\mathcal{P}$ the parcel saturation pressure difference and p the parcel level or data pressure level to distinguish it from the Saturation Level, p_{SL}. The procedure we shall use is to analyze parcel processes, including cloud–environment mixing and diabatic processes in terms of their Saturation Point. This is a shift to a (T_{SL}, p_{SL}, p) coordinate system for the three independent parcel variables, from (T, p, q) or (θ_L, θ_E, p). If parcel $p \neq p_{SL}$, the non-conservative parcel properties such as T, q_S, l, T_W, etc., can be recovered as in Fig. 1 by drawing the dry and moist adiabats and line of constant q through the *SP* to parcel pressure p.

The general thermodynamic relationships between dry adiabat, moist adiabat, and the saturation mixing ratio lines are given in the Appendix, together with a more general notation for the symbols in Fig. 1.

c. *Saturation Point structure of a sounding*

A conventional sounding can be plotted on a thermodynamic diagram in terms of the SP of the atmosphere rather than (T, T_D, p). Radiosondes do not measure liquid water, so if they pass through cloud, the true SP is not measured, but in unsaturated air, it is straightforward to find the LCL, and plot (T_{SL}, p_{SL}) labeled with the pressure p of the data level. Fig. 2 shows a conventional sounding together with this alternative representation. Following Rossby (1932) we may regard the SP profile as a *characteristic curve* for the atmospheric thermodynamic structure. Well-mixed layers such as the subcloud layer would have a single SP, but in general the thermodynamic structure of a convective layer shows a profile of SP. The dashed line on Fig. 2 is an illustrative *mixing line* (see Section 2e) between the SP's of air from 864 and 603 mb: it is drawn for comparison with later examples.

d. *Irreversible diabatic processes and the Saturation Point*

The significance of the SP for an air parcel is that it does not change during reversible adiabatic ascent or descent: that is, following a parcel

$$\frac{Dp_{SL}}{Dt} = \frac{D\theta_{SL}}{Dt} = \frac{D\theta_{ESL}}{Dt} = \frac{Dq_{SL}}{Dt} = 0. \tag{6}$$

In this sense the SP can be regarded as a thermodynamic tracer for an air parcel. All that changes

as parcel pressure changes is the saturation pressure difference, $\mathcal{P}$, and the non-conserved parameters, such as (T, T_W, T_D) or (T_L, T, T_{DT}). Certain irreversible diabatic process will, however, change the SP and we summarize them here in Fig. 3.

Fallout of precipitation moves the *SP* up the moist adiabat. The air parcel θ_{ESL} does not change, but θ_{SL}, q_{SL} do, as l decreases. For the special case of an air parcel at constant pressure, the parcel (T, p) remains constant as T_L, T_{DT} both approach T, while maintaining the relationship (as l and $\mathcal{P} \rightarrow 0$)

$$C_p(T - T_L) = Ll. \qquad \text{(A12')}$$

This is exactly analogous to the evaporation of falling precipitation into unsaturated air which moves the SP down the moist adiabat: again the parcel θ_{ESL} does not change, while θ_{SL}, q_{SL} do. If the parcel is at constant pressure, the T, T_D both approach the wet-bulb temperature T_W which remains constant, and $|\mathcal{P}|$ decreases toward zero. The relationship (A12) is maintained, as T, T_D change towards T_W

$$C_p(T - T_W) = L(q_W - q) \qquad \text{(A12)}$$

If the parcel pressure changes during the evaporation process, the behavior of the SP remains the same, although the parcel saturation pressure difference $\mathcal{P}$ changes, and with it T, T_W, T_D, although (A12) is still satisfied. Betts and Silva Dias (1979) discussed this process in detail.

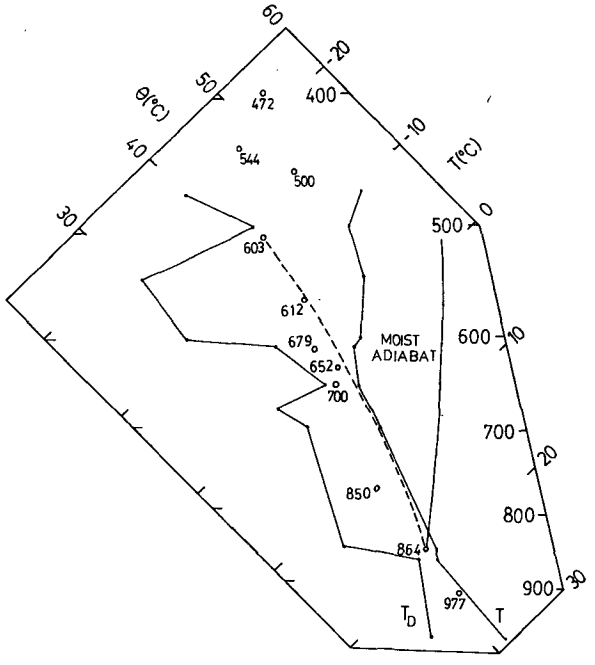

FIG. 2. 1800 Z sounding on 19 July 1977 at Pittsburgh showing conventional plot of $T(p)$, $T_D(p)$ as solid lines, and Saturation Points (T_{SL}, p_{SL}) as open circles, labeled with data pressure level p. The dashed line is an illustrative mixing line between the SP's of 603 mb air and 864 mb air.

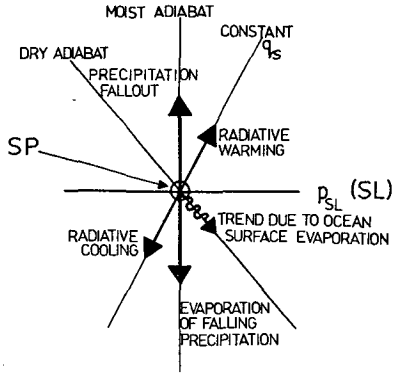

FIG. 3. Schematic showing change in saturation point produced by the irreversible diabatic processes of precipitation fallout or evaporation; radiative cooling or heating; and the tendency caused by ocean surface evaporation.

Radiative processes change the temperature, but not the mixing ratio, so that θ_{ESL}, θ_{SL} change, while q_{SL} remains constant (see Fig. 3). In the free atmosphere there are no processes which change q_{SL}, while conserving θ_{SL}, although at the ocean surface this is the trend produced by the evaporation of water, using the stored sensible heat of the ocean. However, in this case the SP (here the LCL of cloud base) stays constant because the vertical advection of water vapor through cloud base balances the surface flux.

Although Fig. 3 is not drawn to scale, the thermodynamic balance of the entire tropical atmosphere can be regarded as a result of the approximate balance of the three processes: ocean surface evaporation, radiative cooling and precipitation fallout.

e. Mixing diagrams and the saturation point

The parcel conserved parameters (θ_{SL}, θ_{ESL}, q_{SL}) are conserved in adiabatic motion and approximately in isobaric mixing processes (Betts, 1973; Deardorff, 1976, 1980). Since the SP characterizes parcel conserved properties, we need only consider their *SP*'s in mixing two parcels. This is a great simplification. For example, if we mix equal masses of air parcel with different SP's (T_{SL1}, p_{SL1}), (T_{SL2}, p_{SL2}), the SP of the mixture at (T_{SLM}, p_{SLM}) has properties given by the simple average of their conserved parameters (to slight approximation)

$$\left.\begin{aligned} \theta_{SLM} &= (\theta_{SL1} + \theta_{SL2})/2 \\ \theta_{ESLM} &= (\theta_{ESL1} + \theta_{ESL2})/2 \\ q_{SLM} &= (q_{SL1} + q_{SL2})/2 \end{aligned}\right\}. \qquad (7)$$

Fig. 4 shows a specific example of mixing between two parcels with saturation points (T_{SL}, p_{SL}) of (20°C, 900 mb) and (5°C, 700 mb). The SP's of *all* mixtures (not just the mixture of equal masses) lie on the dashed *mixing line*, which can easily be constructed on a thermodynamic diagram by computing

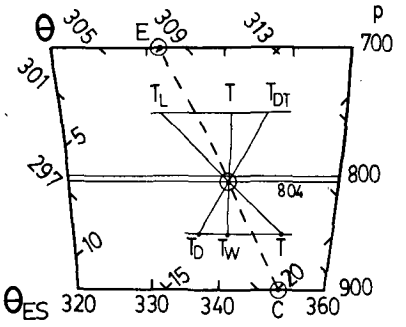

FIG. 4. Tephigram showing mixing between parcels with *SP*'s at *C* and *E* (circled). All mixtures have *SP*'s on the dashed mixing line. The 1:1 mixture has $SP\,(T_{SL}, p_{SL})$ at (13.5°C, 804 mb) shown. This gives its conserved parameters: Its parcel properties at other pressure levels are given by the construction shown.

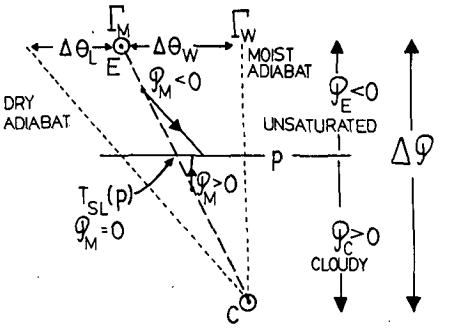

FIG. 5. Schematic mixing diagram for two parcels, one cloudy, one unsaturated (environmental), showing mixing line (heavy dashes) with a gradient between dry and moist adiabats. The construction of the temperature at a pressure level p is shown for mixtures with *SP*'s on the mixing line. The mixture with *SL*, $p_{SL} = p$, is just saturated with $l = 0$. Its temperature $T_{SL}(p)$ is the coldest of all cloud-environment mixtures at that pressure level p.

θ_{SL}, q_{SL} for different mixtures and finding their associated *SP*. Table 1 shows the computation for several mixtures.

The distinction between the *saturation level* of a parcel p_{SL} and the *data pressure level* p, where a parcel may find itself in the atmosphere, is of crucial importance. The tephigram is being used to represent *both*. For example, suppose we consider a mixing process at 800 mb between cloudy air which has risen adiabatically from cloud base at 900 mb where it had the SP at C shown. Its SP has stayed at C, while $\mathcal{P} = p_{SL} - p$ has become positive and its liquid water has increased (A5′). This cloudy air mixes isobarically at 800 mb with air that has an SP at E (unsaturated environmental air, for example, which could have originated at 800 mb or descended adiabatically from any other level). All the mixtures of C and E have SP's on the dashed line. The mixtures that are unsaturated have a saturation level $p_{SL} < 800$ mb, corresponding to $\mathcal{P} < 0$, while the mixtures that are cloudy are those which have $p_{SL} > 800$ mb. The 1:1 mixture in Table 1, for example, with *SL* at 804 mb, is only just cloudy at 800 mb; if it sinks to pressures above 804 mb, it becomes unsaturated. Its (T, T_W, T_D) or (T_L, T, T_{DT}) at any other pressure level are found by drawing dry and moist adiabats and constant q_S lines through its SP as shown (the same construction as in Fig. 1).

The dashed line, representing the SL's and SP's of all mixtures (of C and E) is *unchanged*, whatever the pressure level of mixing; although for every mixture $\mathcal{P}$ changes as p changes.

It is clear that it is easy to find with this diagram the temperature, humidity, liquid water content, etc., of any mixture at any pressure level. Thus, comparisons of cloud–environment mixtures with sounding properties can be made (Sections 3b, 4c).

The mixing line on a tephigram is slightly curved because of the unequal spacing of the q_S and θ_{ES} lines (e.g., see Fig. 2). Table 1 shows, for example, that for the 1:1 mixture $p_{SLM} > \frac{1}{2}[p_{SL}(C) + p_{SL}(E)]$ by ~4 mb. Nonetheless, for qualitative purposes and for mixing lines between SP's which are not too far apart (in p_{SL} or θ_{ESL}), the SL of mixtures can be approximately found by simple averaging of values of p_{SL} or $\mathcal{P}$.

TABLE 1. Mixing of two parcels C and E in various mass ratios.

Parcel	P_{SL}	T_{SL}	θ_{SL}	q_{SL}	θ_{ESL}
C	900	20.0	302.1	16.6	351.3
E	700	5.0	308.0	7.9	332.0
Mixture					
1:3	754	9.6	306.5	10.0	336.9
1:1	804	13.5	305.1	12.2	341.7
3:1	853	17.0	303.6	14.4	346.5

f. Slope of the mixing line

This analysis of the mixing of two parcels in terms of the mixing line between their SP's is particularly useful for convective systems where there are essentially two different "source regions" of air with distinct properties. Among the examples to be explored later (Sections 5, 6) are stratocumulus and the trade cumulus layer where warm dry air is subsiding into a well-mixed layer, and severe storms where the surface well-mixed layer is overlain by a nearly dry adiabatic layer of higher θ which had its source elsewhere in a mixed layer usually over drier elevated terrain. An important parameter for stability questions is the slope of the mixing line in relation to the dry and moist adiabats, and the slope of the θ_v isopleths (see Section 4).

To the linear approximation the mixing line gradient is a function only of the SP's of the two source regions. Fig. 5 defines this gradient $\Gamma_M = \partial\theta/\partial p$ for the mixing line in relation to the slope of the moist

adiabat $\Gamma_W = (\partial\theta/\partial p)_{\theta_{ES}}$.

$$\Gamma_M = \frac{\Delta\theta_L}{\Delta\mathcal{P}} = \left(\frac{\Delta\theta_L}{\Delta\theta_L + \Delta\theta_W}\right)\Gamma_W, \qquad (8)$$

where, as shown,

$$\Delta\mathcal{P} = \mathcal{P}_C - \mathcal{P}_E,$$

$$\Delta\theta_L = \theta_{SL}(C) - \theta_{SL}(E),$$

$$\Delta\theta_W = \theta_W(E) - \theta_W(C).$$

(See Table 4 for notation.) An essentially identical relationship exists for the mixing line gradient in θ_{ES} coordinates in terms of $(\partial\theta_{ES}/\partial p)_\theta$.

Fig. 5 shows a mixing process typical of shallow cumulus, where Γ_M lies between wet and dry adiabats. For stratocumulus cloud-top mixing, $|\Delta\theta_W| \ll |\Delta\theta_L|$, and Γ_M approaches Γ_W (see Section 5a) Paluch (personal communication, 1980) has mathematically derived the mixing line gradient. Fig. 5 is a simple graphical representation.

3. Mixing in cumulus clouds

The mixing line analysis (Fig. 5) can be used to formulate many cumulus mixing processes. Two schematic examples are presented.

a. Minimum temperature from cloud–clear air evaporative mixing

Fig. 5 elegantly solves the well-known problem of the equilibrium temperature of cloud–environment mixtures. For the mixture with SP where the mixing line crosses any pressure level p, $p = p_{SL}$ and $\mathcal{P}_M = 0$. This is by definition the mixture that is just saturated with no liquid water at the pressure level p, with temperature $T_{SL}(p)$. The temperature of mixtures that have SL's away from p are found by drawing dry adiabats (for unsaturated mixtures $\mathcal{P}_M < 0$) or moist adiabats (for cloudy mixtures $\mathcal{P}_M > 0$) from the mixing line back to p, as shown in Fig. 5. It is obvious that provided the mixing line lies between dry and moist adiabats, then the just saturated mixture has the minimum temperature $T_{SL}(p)$. The θ depression of $T_{SL}(p)$ below that of the environment is given by

$$\Delta\theta = -\Delta\theta_L\mathcal{P}_E/(\mathcal{P}_C - \mathcal{P}_E) \approx (1 - \sigma)\Delta\theta_L, \qquad (9)$$

where σ is the fraction of environment in this just saturated mixture. The water budget for this mixture, the use of the Clausius-Clapyron relationship and a little algebra gives the familiar formula for the ratio of environment to cloud which just evaporates all the cloud water (e.g., Ludlam, 1980, p. 55)

$$\frac{\sigma}{1 - \sigma} = (1 + \gamma)l_C/(q_S - q)_E, \qquad (10)$$

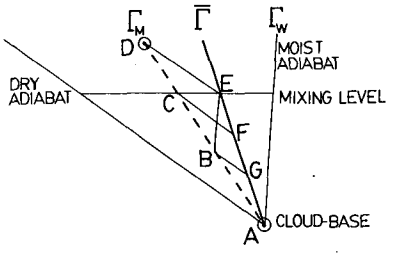

FIG. 6. Construction of thermal equilibrium level of mixtures given the mixing line and an environmental sounding. G is the lowest equilibrium level of a mixture that is negatively buoyant at E (ignoring the virtual temperature correction).

where $\gamma = L^2q_S|C_pR_vT^2$ [see (A18)], l_C is the cloud water content, and $(q_S - q)_E$ the saturation deficit of the environment.

b. Cumulus mixing and downdraft equilibrium level

A comparison of the mixing line (Fig. 5) with the environmental stratification is clearly of great significance. Certain mixtures will be colder than the environment and will tend to form downdrafts; others will be warmer and might be expected to characterize updrafts. The problem is first treated here in an idealized manner with linearized lapse-rates and without the virtual temperature correction (see Section 4).

Fig. 6 shows a schematic tephigram with dry and moist adiabats, an environmental stratification $\bar{\Gamma}$, and a mixing line between cloudy air which has risen undiluted from cloud-base at A and environmental air at the mixing level, which is unsaturated, with SP at D. DE, CF, BG are dry adiabats, and EB is a moist adiabat. All the cloud–environment mixtures have SP's on AD, which may be categorized as follows:

Mixtures with SP's:

1) Between D and C are unsaturated, cooler than the environmental $\theta(E)$ and may sink to equilibrium between E and F (ignoring the virtual temperature correction).

2) At C, is just saturated, has a minimum temperature and an equilibrium level F.

3) Between C and B are saturated and cloudy, cooler than the environment $\theta(E)$ and may sink, first moist adiabatically to their SP, and then along a dry adiabat to thermal equilibrium between F and G.

4) At B, this parcel has the same potential temperature as the environment at E, and the same θ_{ES}.

5) Between B and A, are cloudy and warmer than the environment and are likely to ascend a moist adiabat.

Thus, from buoyancy considerations alone (ignoring until Section 4 the θ_v correction) one might expect

mixture properties on DC to be characteristic of unsaturated downdrafts, on CB of cloudy downdrafts, and on BA of cloudy updrafts.

Fig. 6 shows that the lowest level that negatively buoyant downdrafts produced by mixing can reach thermal equilibrium is G, considerably above cloud base (see Fraser, 1968; Betts, 1973). This level is of theoretical significance.

c. *Lowest downdraft equilibrium level*

A formula for G in Fig. 6 (which may be thought of as the lowest downdraft equilibrium level) can be derived geometrically using the linearized lapse-rates. Let

$$\sigma = \frac{\mathrm{AG}}{\mathrm{AE}} = \frac{\mathrm{AB}}{\mathrm{AD}} = \frac{\mathcal{P}_A - \mathcal{P}_B}{\mathcal{P}_A - \mathcal{P}_D}. \tag{11}$$

The letter subscripts denote values of the saturation pressure difference for that point, simply the pressure difference from the mixing level at E. σ is both the ratio AG/AE and the (approximate) fraction of environmental air contributing to the critical mixture B (see Section 3a). $\mathcal{P}_A$, $\mathcal{P}_B$, $\mathcal{P}_D$ can be eliminated from (11) using the identities

$$\theta(A) - \theta(E) = \bar{\Gamma}\mathcal{P}_A = \Gamma_M(\mathcal{P}_A - \mathcal{P}_D),$$

$$\theta(B) - \theta(E) = \Gamma_W\mathcal{P}_B = \Gamma_M(\mathcal{P}_B - \mathcal{P}_D),$$

where $\theta(A)$ denotes θ at the point A on the tephigram, to give

$$\sigma = \frac{\Gamma_M(\Gamma_W - \bar{\Gamma})}{\bar{\Gamma}(\Gamma_W - \Gamma_M)} = \frac{\mu(1-\eta)}{1-\eta\mu}, \tag{12}$$

where $\mu = \Gamma_M/\bar{\Gamma}$, $\eta = \bar{\Gamma}/\Gamma_W$. $\sigma = 1$ corresponds with no descent, while $\sigma = 0$ corresponds to descent to cloud-base:

1) For $\mu \geqslant 1$, no descent is possible, as is clear from Fig. 6;
2) As $\mu \to 1$ ($\Gamma_M \to \bar{\Gamma}$), $\sigma \to 1$;
3) As $\eta \to 1$ ($\bar{\Gamma} \to \Gamma_W$) and $\mu < 1$, $\sigma \to 0$;
4) As $\mu \to 0$ (Γ_M towards the dry adiabat), $\sigma \to 0$.

Both 3) and 4) are cases favoring descent to cloud-base. Case 3) corresponds qualitatively to the stratocumulus layer where negatively buoyant cloudy downdrafts are possible from mixing processes (Lilly, 1968; Deardorff, 1980; Randall, 1980). This case is discussed more fully in Section 5. Case 4) has a rough correspondence with the severe storm atmosphere where both Γ_M, $\bar{\Gamma}$ approach the dry adiabat and negatively buoyant unsaturated downdrafts are readily formed by mixing processes. However, the real case is more complex than Fig. 6 (see Sections 5, 6). In addition, in both types of mixing instability the virtual temperature correction is important (see next section).

Typically, cumulus convection is an intermediate case, with Γ_M and Γ midway between dry and moist adiabats in the lower cumulus layer. Typically, air can sink part-way back towards cloud-base (Betts, 1973; Fraser, 1968).

In general, Fig. 6, though oversimplified, suggests the instability criterion for negatively buoyant downdrafts from mixing is: $\mu < 1$, or $|\Gamma_M| < |\bar{\Gamma}|$. We shall see in Section 6 that some convective atmospheres attempt to establish an equilibrium structure in which $\Gamma_M \approx \bar{\Gamma}$.

4. Virtual potential temperature

The virtual temperature correction is important for instability and buoyancy equilibrium analyses. Deardorff (1980) has shown how isopleths of virtual potential temperature θ_v, given by

$$\theta_{vu} = \theta(1 + 0.61q), \tag{13a}$$

$$\theta_{vc} = \theta(1 + 0.61q_S - l), \tag{13b}$$

for unsaturated and cloudy air, respectively, can be drawn on (θ_L, q_T) buoyancy mixing diagrams: (θ_{SL}, q_{SL}) in our notation. The advantage of these diagrams is that mixing lines are exactly straight. The disadvantage is that they must be drawn for each pressure level. Conversely, the tephigram analysis used here shows all pressure levels and (conceptually) all mixtures simultaneously, although the mixing lines are curved, and θ_v isopleths are not conventionally plotted.

a. *Tephigram plot of* θ_v

θ_v overlays can however be drawn for a tephigram for any parcel pressure level p [and a stability analysis identical to that of Deardorff (1980)]. The value of θ_v is read at the SP (T_{SL}, p_{SL}) not (T, p). We shall find that qualitatively a single overlay depicts the shape of the θ_v isopleths for a range of parcel pressure p. The distinction between parcel p and saturation level p_{SL} is again crucial. We may rewrite (13a), (13b) to make this clearer.

$$\theta_{vu}(p_{SL}) = \theta_{SL}(1 + 0.61q_{SL}), \tag{13a'}$$

$$\theta_{vc}(p_{SL}, p) = \theta(p)[1 + 0.61q_S(p) - l(\mathcal{P})], \tag{13b'}$$

where

$$\mathcal{P} = p_{SL} - p \text{ is here positive.}$$

For unsaturated air, θ_{vu} is a unique function of (T_{SL}, p_{SL}) at the SP, so isopleths of θ_v can be drawn on a thermodynamic diagram, with the convention that θ_v is read at the SP. For cloudy air, θ_{vc} depends on θ, q_S which are defined at p, and l which increases as $\mathcal{P} = p_{SL} - p$ increases. Specifically, this means that the θ_v isopleths appropriate to a given parcel pressure level p, kink at p (where $\mathcal{P} = 0$), since parcels with $p_{SL} < p$ are unsaturated and for them $\theta(p)$

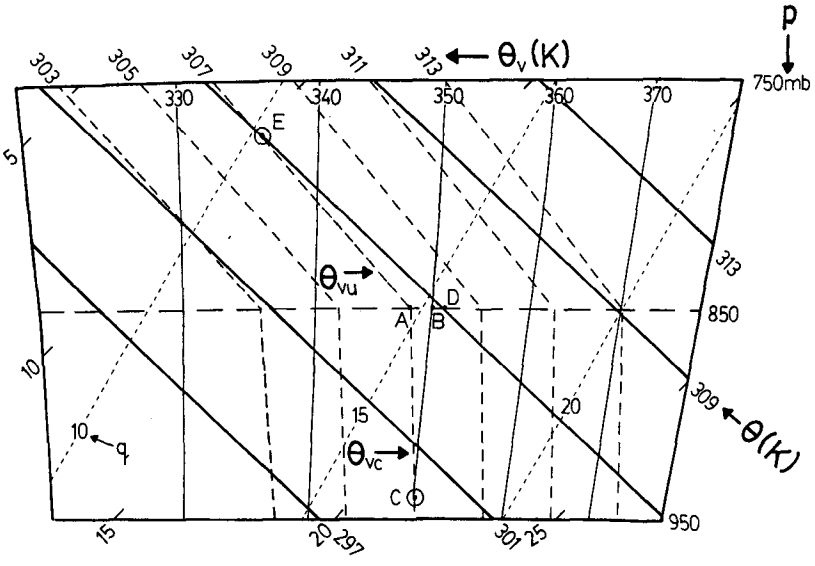

FIG. 7. Section of tephigram showing isopleths of θ_v (heavy dashed, in K) for a parcel level of 850 mb. The parcels with saturation points at C (cloudy) and E (unsaturated environment) have the same θ_v, although the environment is warmer. The light dashed lines are saturation mixing ratio.

$= \theta_{SL}$, $q(p) = q_{SL}$. Parcels with $p_{SL} > p$ ($\mathcal{P} > 0$) are cloudy, and their $\theta(p)$, $q_S(p)$ lie on the moist adiabat through the SP.

Fig. 7 shows a section of a low-level tephigram with θ_v isopleths (heavy dashes) overlaid for a parcel level of 850 mb (i.e. $\mathcal{P} = 0$ at 850 mb). If we plot the SP of an air parcel which is at 850 mb, the dashed lines give its θ_v. For SL's below 850 mb (the "*unsaturated region*" with respect to the given data level of 850 mb) θ_{vu} increases along the dry adiabat ED (for example) as the saturation mixing ratio ($q_S = q_{SL}$) rises. For pressures above p, SP's on the moist adiabat BC (the "*cloudy region*" with respect to 850 mb) have the same θ, q_S at point B but increasing cloud liquid water l with a corresponding increase of $\mathcal{P}$, decrease of θ_L. θ_{vc} thus decreases as l increases on BC (Eq. 13b′).

The moist adiabat BC ($\theta_{ES} = 350$ K) intersects the $\theta_v = 307$ K isopleth at C, and the dry adiabat DE intersects the same isopleth at E. Thus, at the data level p, cloudy and environmental parcels which have SP's at C, E respectively have the same buoyancy, although the environmental parcel is actually warmer $\theta(D) > \theta(B)$: the negative contribution to buoyancy of l does not, in this case, offset the greater cloud water vapor. Cloudy parcels with SP's on BC are positively buoyant with respect to the environment (SP at E), while those with SP's lower than C are negatively buoyant because of their greater l.

If an air parcel moves from 850 mb dry or moist adiabatically to another pressure level p its SP does not change, but the θ_v isopleths now kink at the new p level. If the parcel is cloudy, its θ (and θ_{vc}) will be different, but if it is unsaturated, neither θ nor θ_{vu} changes.

In fact, an overlay of simply the dashed lines on Fig. 7 (with q_S labeled and θ_v unlabeled) is of practical use because it shows the slope of the θ_v isopleths in both cloudy and unsaturated regions (with respect to a data pressure level p), since the isopleths depend predominantly on the q_S field. One aligns the correct q_S isopleths and the kink at $\mathcal{P} = 0$ with a data p level. The labeling shown of the θ_v isopleths is only valid with $\mathcal{P} = 0$ at 850 mb, but the shape of the isopleths is sufficiently accurate for diagrammatic uses (see Section 5) over a wide range of data levels (750–950 mb).

b. Relation of θ_v isopleths to dry and moist adiabats

The slope of the θ_v isopleths and their deviation from the dry and moist adiabats is of importance to stability analyses. It is informative to express these as fractions of the slope of the moist adiabat

$$\Gamma_W = (\partial\theta/\partial p)_{\theta_{ES}} . \qquad (14)$$

Simple linearized expressions are derived in Section *c* of the Appendix.

1) UNSATURATED REGION: $\mathcal{P} < 0$

The gradient of the θ_{vu} isopleth can be written

$$\left(\frac{\partial\theta_{SL}}{\partial p_{SL}}\right)_{\theta_{vu}} = \beta_1\Gamma_W . \qquad (A25)$$

Table 2 lists values of the coefficient β_1, which in-

TABLE 2. Coefficients in slope of θ_v isopleths (at 900mb) (pressure variation is small).

q_S (g kg^{-1})	1	5	10	15	20	25
β_1	0.07	0.12	0.17	0.21	0.24	0.27
β_2	0.10	0.11	0.11	0.10	0.10	0.09

creases with the saturation mixing ratio, q_S. For moist atmospheres, characteristic of the tropical oceans, $\beta_1 \approx 0.2$, which means that the slope of the θ_{vu} isopleth is a small but not negligible fraction of the moist adiabat.

2) CLOUDY REGION: $\mathcal{P} > 0$

A similar analysis for the saturated, cloudy region, shows that the isopleths deviate from the moist adiabat by a nearly constant fraction of the slope of Γ_W

$$\Gamma_W - \left(\frac{\partial\theta_{SL}}{\partial p_{SL}}\right)_{\theta_{vc},p} = \beta_2\Gamma_W \approx 0.1\Gamma_W. \quad \text{(A30)}$$

In this case the coefficient β_2 is nearly constant (Table 2), because both the slope of the θ_{vc} isopleth and the moist adiabat are related to $(\partial q_S/\partial p)_{\theta_{ES}}$.

The slope of the θ_{vc} isopleth gives the criterion for cloud-top entrainment instability for a stratocumulus layer (see Section 5a). This slope is also of significance to cloud parcel buoyancy. Although an ascending cloud parcel θ may follow the moist adiabat

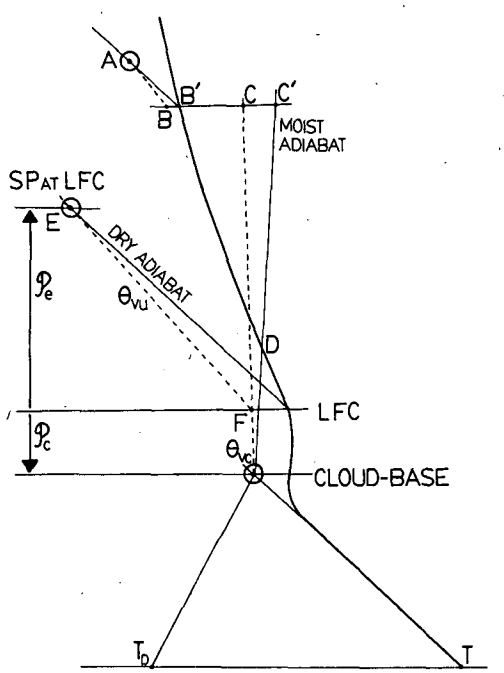

FIG. 8. Schematic showing use of θ_v construction (short dashes) to determine parcel buoyancy, and level of free convection.

Γ_W, its *buoyancy* is effectively following a θ_{vc} isopleth of only $0.9\Gamma_W$, a considerable reduction in buoyancy (see Section 6), until cloud water is converted to precipitation water and falls out.

Using (A19) and (A20), we may write (A30) in terms of the θ_{ES} gradients on the θ_{vc} isopleth and the dry adiabat

$$\left(\frac{\partial\theta_{ESL}}{\partial p_{SL}}\right)_{\theta_{vc},p} \approx 0.1\left(\frac{\partial\theta_{ES}}{\partial p}\right)_{\theta}. \quad \text{(15)}$$

c. Parcel buoyancy, convective available potential energy (CAPE), and level of free convection (LFC)

Since the θ_v correction markedly affects parcel buoyancy, several conventional tephigram definitions of cloud parcel parameters are affected significantly.

Fig. 8 shows the modified construction of parcel buoyancy, CAPE (Moncrieff and Miller, 1976), and LFC. Two extremes are shown. At a level well above cloud-base, a parcel that has ascended moist adiabatically to C', without fallout of cloud water[1], has a buoyancy equivalent to a saturated parcel at C on the θ_{vc} isopleth through the cloud-base SP. The unsaturated environment, with SP at A, has a buoyancy equivalent to a saturated parcel (with $l = 0$) at B on the θ_{vu} isopleth through A. Thus the cloud–environment buoyancy is proportional to BC, not B'C'[$\delta\theta \propto \delta\theta_v$: see (A23)]. For a nearly saturated tropical atmosphere, the correction CC' is large (see Sections 6e, 6f), in comparison to BB' and CAPE is approximately proportional to the area between the sounding curve and the θ_{vc} isopleth, not the moist adiabat. As microphysical processes convert cloud water to precipitation particles which fall out, the θ_v of cloud parcels returns closer to the moist adiabat, as their SP changes.

Near cloud-base a similar construction affects the definition of the LFC. The LFC is usually defined as the level D (Fig. 8) where a moist adiabat through cloud-base intersects the sounding temperature curve: so that cloud parcels are buoyant above this level. In fact, the LFC is not at D but at level F, where cloud parcel and environment have the same θ_v. At F the θ_{vu} isopleth through the environment SP intersects the θ_{vc} isopleth through the cloud-base SP. Typically, the LFC is near cloudbase and the correction for liquid water content is small. But for warmer temperatures (see coefficients in Table 2) or dry environments, the deviation of the θ_{vu} isopleth from the dry adiabat produces a significant lowering of the LFC over that computed on the basis of θ alone: see Fig. 8 and Section 6b.

[1] For a few-hundred mb, above cloud-base, the difference between the pseudo-adiabat and reversible adiabat temperature curves is small (see Saunders, 1957) compared with the θ_{vc} correction.

5. Idealized examples of evaporative mixing instability

Using the mixing analysis of Section 2f and the θ_v tephigram representation (Section 4), we now discuss and contrast three widely different convective regimes: stratocumulus, cumulus and the severe storm environment. As mentioned earlier, the Saturation Point and mixing line approach is particularly useful for the mixing of two distinct air masses.

a. Stratocumulus instability on a tephigram

In a stratocumulus layer, warmer drier air is subsiding into a cloud-filled mixed layer which is itself in equilibrium with the underlying dry adiabatic layer near the surface. The structure of the layer and the properties of the ascending and descending branches of the circulation within it are determined by several processes, including the radiative flux divergence at cloud-top, the surface fluxes, and the entrainment or mixing of the warm dry air above the inversion with air that originates in the unsaturated mixed layer above the surface [see, for example, Lilly (1968), Deardorff (1976), Betts (1978), Schubert *et al.* (1979)]. The evaporative mixing at cloud-top, though only one of several processes involved, is believed to be important.

Several authors have discussed the instability of a stratocumulus layer which results from cloud-top mixing if the θ_E of air above the inversion is low enough. Lilly (1968) suggested that the condition for the breakup of a layer by this instability was that θ_E should decrease across the capping inversions ($\Delta\theta_E < 0$). Randall (1980) and Deardorff (1980) have extended this analysis to include virtual temperature effects and have shown that the criterion for instability is more stringent and requires a still lower θ_E above the inversion

$$\Delta\theta_E < (\Delta\theta_E)_{\text{crit}} \quad \text{where} \quad (\Delta\theta_E)_{\text{crit}} \approx -1 \text{ to } -2 \text{ K}.$$

They show that it is the virtual temperature correction due to the liquid water that tends to make stratocumulus more stable to entrainment instability.

The tephigram mixing diagram analysis shows this same criterion in terms of $\Delta\theta_E$, $\Delta\mathcal{P}$ (between cloud and clear air). The critical criterion for instability then becomes very simply a comparison of the slope $\Delta\theta_E/\Delta\mathcal{P}$ and that of the θ_{vc} isopleths in the cloudy region (as in Deardorff, 1980). This permits easy comparison with other convective regimes. Fig. 9 shows the construction.

The dry and moist adiabats drawn as heavy solid lines correspond to properties of air in the ascending branch of the stratocumulus circulation. Cloudy air reaches the inversion at cloud-top with θ_C shown, but retains an SP at cloud-base. It mixes at cloud top with warm dry air (θ^+, q^+) above the inversion with

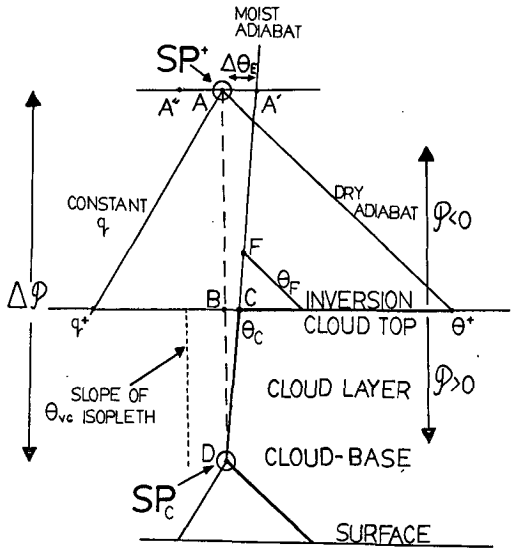

FIG. 9. Schematic tephigram for stratocumulus cloud-top entrainment instability. Heavy line is sounding in ascending air through dry adiabatic layer and moist adiabatic cloud layer, capped by a strong inversion at cloud-top. Saturation points SP_c for ascending cloudy air (corresponding to LCL at cloud-base) and warm dry air just above inversion (SP^+), with the missing line between them (heavy dashed line). The critical mixing line for instability is drawn which is parallel to the θ_{vc} isopleth (short dashes) in the cloudy region ($\mathcal{P} > 0$).

an SP^+ as shown. The heavy dashed mixing line (AD) is parallel to the θ_{vc} isopleth, which means that all cloudy mixtures with SP's on BD have exactly the same buoyancy as the ascending unmixed cloudy air. We can see that AD must be the critical mixing line dividing stability and instability of cloudy mixtures by considering the points A′ and A″.

If the air above the inversion had SP at A′, then all mixtures would have SP's on the moist adiabat shown. It is clear that unsaturated mixtures ($\mathcal{P} < 0$), such as F, are warmer than the cloud ($\theta_F > \theta_C$) and cannot sink into the cloud. The cloudy saturated mixtures with SP's on CD all have the same θ_C, but a greater θ_{vc} than unmixed cloudy air, because their liquid water content l is less. Thus, mixtures with A′ air would be stable and not sink into the cloud (ignoring the large radiative cooling which cools cloud-top air parcels and mixtures, thus driving the descending branch even in this stable case).

Correspondingly, cloudy mixtures ($\mathcal{P} > 0$) with A″ air are unstable because they have a θ_{vc} cooler than the unmixed cloudy air, since their mixing line is to the left of the θ_{vc} isopleth through cloud-base. These mixtures can sink freely into the cloud layer as negatively buoyant, saturated downdrafts until they run out of cloud water at their saturation level. An important aspect of this process is that the mixing of only a little dry air with SP at A″ produces a negatively buoyant mixture, since *all* cloudy mix-

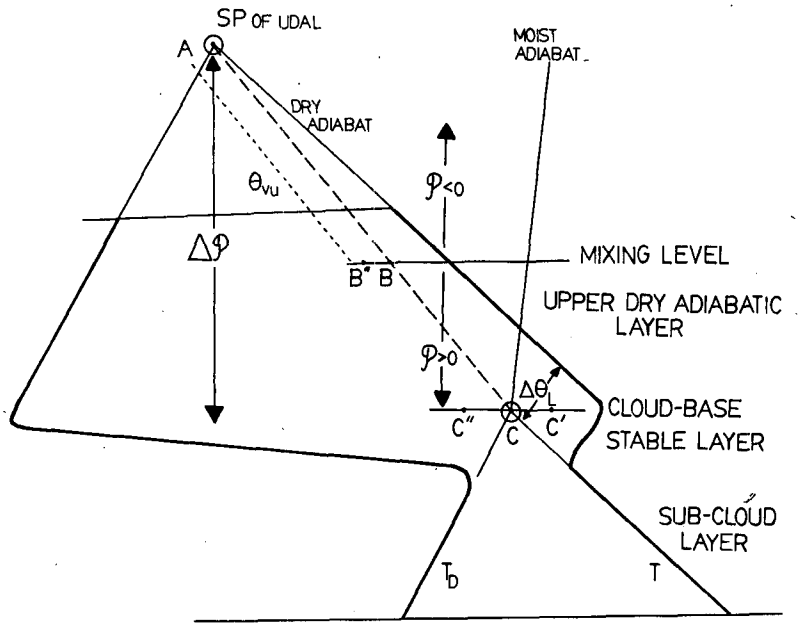

FIG. 10. Schematic tephigram for the formation of unsaturated downdrafts in the severe storm environment. The idealized sounding of T, T_D (heavy lines) shows warm upper dry adiabatic layer (UDAL) overlying moister subcloud layer. Saturation points are shown for the two layers and the mixing line AC between them (heavy dashes). The mixing line drawn is the critical mixing line for instability, which is parallel to the θ_{vu} isopleth (short dashes) in the unsaturated region ($\mathcal{P} < 0$).

tures are negatively buoyant if the mixing line is to the left of the θ_{vc} isopleth [contrast (5b) for a severe storm environment].

Thus, the critical condition for instability in terms of jumps across the inversion can be written (using linearized gradients)

$$\frac{\Delta\theta_E}{\Delta\mathcal{P}} > \left(\frac{\partial\theta_{ESL}}{\partial p_{SL}}\right)_{\theta_{vc},p} \approx 0.1\left(\frac{\partial\theta_{ES}}{\partial p}\right)_{\theta}, \qquad (16)$$

using (15). In this form the critical condition is easily visualized on a tephigram: it is to the left of the moist adiabat through cloud-base by $^1/_{10}$ of the difference in slope between dry and moist adiabats. The coefficient is largely independent of pressure and temperature (Table 2).

The criterion derived by Randall (1980) and Deardorff (1980) is essentially equivalent to (16). Eq. 12b of Deardorff (1980) corresponds to finding $(\partial\theta_{ESL}/\partial q_{SL})_{\theta_{vc}}$ on AC in our Fig. 7. The usefulness of (16) is that it is readily visualized on a routine sounding.

If (16) is satisfied, one would expect a stratocumulus layer to break up; conversely, scattered cumulus layers such as trade cumulus presumably satisfy the instability criterion (Randall, 1980) (an example is shown in Section 6d). Since (16) is simply a comparison of the SP's of the subcloud mixed layer and warm dry air at inversion top, and since typically θ_E decreases with height in the atmosphere, we see that the presence of stratocumulus requires that (16) be not satisfied, implying processes that produce relatively:

1) High θ_E above the inversion, such as strong sinking outweighing radiative cooling, or
2) Low θ_E in the surface layer, such as advection over cooler land or ocean.

The magnitude of $\Delta\mathcal{P}$ can be regarded as of quantitative importance in determining the magnitude of the critical $\Delta\theta_E$ in (16).

As Randall (1980), Deardorff (1980) and Moeng and Arakawa (1980) conclude, the breakup of a stratocumulus layer will occur if the air is advected over a warmer surface or into a region of weaker large-scale subsidence.

b. Unstable downdrafts in the severe storm environment

The severe storm environment provides fascinating parallels and contrasts with the stratocumulus layer. Fig. 10 shows an idealized structure of a conditionally unstable storm environment with a deep potentially warm dry adiabatic well-mixed layer overlying a cooler moister dry adiabatic layer near the surface. This is a characteristic structure for the formation of severe storms (see, for example, Ludlam, 1980,

Chapter 8.7). The upper dry adiabatic layer (UDAL) typically originates as a deep mixed layer over an arid elevated terrain, and provides a strong capping inversion for the underlying moister boundary layer. However, if deep convection is triggered by intermediate-scale circulations, the UDAL provides a highly unstable environment for severe storm growth. It is also highly unstable for downdraft circulations. Kamburova and Ludlam (1966) and Betts and Silva Dias (1979) have discussed the formation of strong downdrafts in a nearly dry adiabatic environment by the evaporation of falling precipitation. Evaporative mixing can also produce strong downdrafts in the UDAL. Whether this process plays any role in severe storm dynamics is not clear: the effect of wind shear and precipitation evaporation may be far more important. However, besides its theoretical significance, it does suggest a mechanism for the triggering of unstable downdrafts in smaller clouds in the early stages of storm development.

Once again, in Fig. 10 we see two overlying air masses characterized by very distinct SP's. Air rising from the well-mixed subcloud layer has an SP at C (its LCL, and cloud-base).

The well-mixed UDAL shown (an idealization) has an SP (its LCL) at A, and the mixing line AC for mixtures between the two air masses is shown (heavy dashes). Mixtures represented by points between A and B are unsaturated, produced by the evaporation of cloud air into the dry environment. Because C has a lower θ_L than θ of the UDAL, these mixtures are colder than the UDAL. However, they are also moister, and for the mixing line shown, which is parallel to the θ_{vu} isopleth for unsaturated air, all unsaturated mixtures are just neutrally buoyant. This is thus the critical mixing line dividing regions of stability and instability. If cloud-base SP were at C′, all unsaturated mixtures are positively buoyant; in fact, the atmosphere has become absolutely unstable because θ_v of the subcloud layer is greater than that of the UDAL (see below). Typically, we would thus expect the SP of cloud-base air to be at C″, so that cloud-base air has a lower θ_v than the UDAL. However this means that all unsaturated mixtures with SP's on AB″ have a lower θ_{vu} than the UDAL, and can sink freely as negatively buoyant downdrafts to the base of the UDAL and perhaps overshoot into the subcloud layer.

This instability can, in a sense, be regarded as the opposite of the stratocumulus case. Here, the evaporative mixing of a little cloud air into the upper dry adiabatic layer produces unstable dry downdrafts, provided the cloudy air (from cloud-base) has a low enough θ_L: whereas for stratocumulus it is the mixing of a little environmental air into the moist adiabatic cloud layer that produces unstable saturated downdrafts, provided the inversion top air has low enough θ_E. In both cases the critical condition involves the slope of the θ_v isopleths, in the unsaturated and cloudy regions respectively. The analog of (16) for Fig. 10 is that the slope of the mixing line for instability

$$\frac{\Delta\theta_L}{\Delta\mathcal{P}} < \left(\frac{\partial\theta_{SL}}{\partial p_{SL}}\right)_{\theta_{vu}} = \beta_1\Gamma_W \qquad (17)$$

from (A25). The coefficient β_1 is $\sim$0.17 for $q_S \sim 10$ g kg^{-1} (see Table 2).

This condition has in fact a simple meaning, which was alluded to above: it is that the cloud-base air has a lower θ_v than the UDAL for downdraft instability

$$\theta_{vu}(\text{cloud-base air}) < \theta_{vu}(\text{UDAL}). \qquad (18)$$

Because cloud water evaporates, the cloud air is in a sense cooled to its θ_L, which is its cloud-base θ (see Section 3a), so that the buoyancy of unsaturated mixtures involves simply an averaging of the θ_v's in (18). (An analogous argument in reverse exists for the stratocumulus case.)

This mixing instability is simply due to the low θ_L of subcloud air. The evaporation of only a little falling precipitation, which lowers the SP of air in the UDAL (Section 2d; Betts and Silva Dias, 1979) along the moist adiabat (through A in Fig. 10), can easily lower θ_{vu} so as to produce downdrafts which can penetrate to the surface: this rather than evaporative mixing is the mechanism responsible for damaging downdrafts in severe storms. Downdrafts from evaporative mixing may play a role, however, in triggering the development of new clouds in the early stages of storm growth and organization.

The conventional definition of the level of free convection (LFC) would be very misleading in Fig. 10. For a cloud-base SP at C, the LFC is actually *at cloud-base*, since cloud-base air and the UDAL have the same θ_v. If the cloud-base SP is at C″ the LFC is above cloud-base: approximately at the intersection of the moist adiabat through C″ with the θ_{vu} isopleth (here the heavy dashed line) through the SP of the UDAL. (See Fig. 8 and Section 6b.)

c. *Downdrafts in a cumulus layer*

The cumulus layer provides an intermediate and more complex case than those in Sections 5a and 5b because the lapse rate is typically midway between moist and dry adiabats. Correspondingly, only roughly equal mixtures of cloud and environment are negatively buoyant and, as was shown in Section 3c, these mixtures can only descend part-way back to cloud base. As an idealized example, Fig. 11 presents a cumulus layer capped by an inversion, and considers mixing of air from above the inversion with cloud-base air. This is an extension of Fig. 6 by the addition of the inversion, a transition layer at cloud base and the schematic θ_v isopleths.

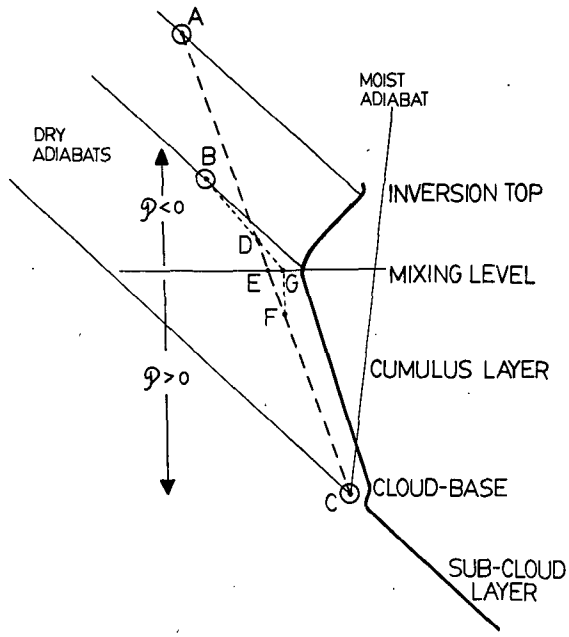

FIG. 11. Schematic tephigram showing possibility of downdrafts from evaporative mixing in a cumulus layer. The heavy line is the environmental T profile. SP's are shown for air from inversion-top (A), mixing level (B) and cloud base (C). The heavy dashed line is the mixing line between cloud base and inversion top, and the light dashed line is the θ_v isopleth through the mixing level SP, at B.

Fig. 11 is a little more complicated than Figs. 9 and 10 because a continuous profile of SP's is involved in the cumulus layer which cannot be idealized to only two. For clarity, though, only three are shown: cloud base, inversion top and the mixing line AC between them and B, the SP for the level of mixing, which is chosen near the inversion base. The mixtures that are negatively buoyant are readily identified by drawing the θ_v isopleth BGF (short dashes) through B, the SP of the level of mixing (since we are comparing buoyancies at this level). This isopleth kinks at the level of mixing, as SP's go from unsaturated to saturated regimes [and θ_v shifts from (13a) to (13b)]. The isopleth also intersects the mixing line AC at D and F. Mixtures with SP on DG are negatively buoyant: on DE they are unsaturated, while on EF they are cloudy. The lowest level to which a mixture can sink corresponds to the equilibrium level of mixture F. This may be found approximately by drawing the dry adiabat through F (as in Fig. 6); more precisely by drawing the θ_{vu} isopleth through F to find the environmental SP with the same θ_v (not shown).

It can be seen that only a limited range of mixtures (of roughly equal masses of cloud and environment for the example shown) can sink freely in negatively buoyant downdrafts and, further, their existence requires that the point E be colder than G.

By comparison to Fig. 6, it is clear that this downdraft instability criterion still corresponds roughly to the mixing line being colder than the environmental sounding, complicated only by the θ_v correction and the colder SP at cloud-base.

Comparing Figs. 9, 10 and 11, we note that if B → A in Fig. 11, this figure simplifies to resemble (apart from environmental lapse rate) the severe storm case Fig. 10, while $B \rightarrow C$ in Fig. 11 corresponds more closely to the stratocumulus case Fig. 9, where the buoyancy comparison is made at the mixing level with air from cloud base.

d. Convective regimes, instability and equilibrium

Fig. 12 summarizes this section in terms of SP structure for the three regimes: stratocumulus, cumulus and severe storm environment, for mixing between cloud-base air and an overlying layer. It also shows schematically the slopes of the θ_{vu}, θ_{vc} isopleths. Clearly this diagram raises the possibility that some classification of convective atmospheres may exist in terms of SP structure. This we cannot explore further here, although a few illustrative examples will be given in Section 6.

In addition, we have so far only examined the question of stability to downdrafts, produced by evaporative mixing. Many convective atmospheres seem to exhibit in some sense a quasi-equilibrium structure (Ludlam, 1966; Betts, 1973; Arakawa and Schubert, 1974; Lord and Arakawa, 1980): that is, in some sense, the atmosphere stratification and the convection are in equilibrium. This is clearly not the case for the onset of a severe storm or the breakup of a stratocumulus layer, but many intermediate cumulus structures do show some tendency to equilibrium. A few examples are given in Section 6.

6. Illustrative examples of instability and convective equilibrium

The theory of the Saturation Point and its use in cloud-mixing processes and tephigram plots of θ_v has

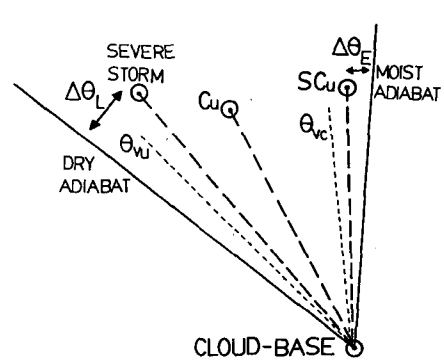

FIG. 12. Schematic summary of *SP* structure for the three convective regimes (heavy dashed lines). The short dashed lines are the schematic slopes of the θ_v isopleths.

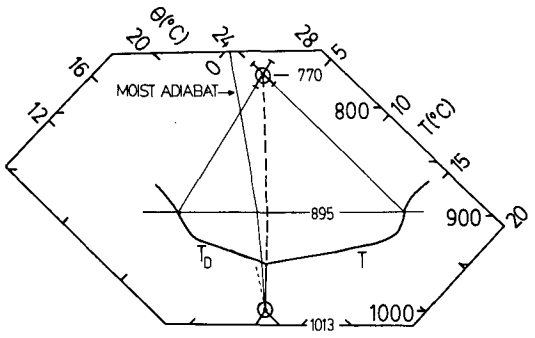

FIG. 13. Aircraft sounding at 1745 Z on 13 June 1976 through stratocumulus layer (33.7°N, 126.5°W). T, T_D soundings are solid lines; saturation points of cloud-base air and a representative inversion top air are shown circled. Error bars on inversion top *SP* are representative of fluctuations of mixing ratio of aircraft observations between 890 and 920 mb. Short dashed line denotes slope of θ_{vc} isopleth through cloud-base SP.

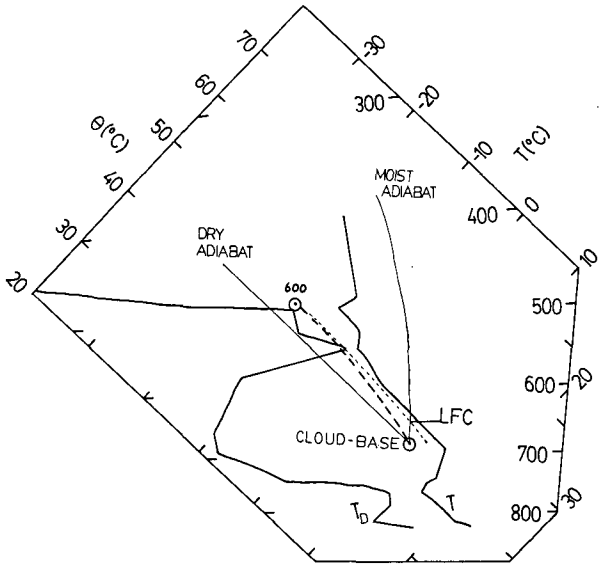

FIG. 14. 1800 Z sounding at Limon (LIC) on 14 August 1977, showing temperature and dewpoint (heavy lines), dry and moist adiabat through cloud base (light lines), mixing line between cloud-base SP and that for 600 mb air (heavy dashes), and θ_{vu} isopleth (light dashes) through the upper environmental SP. The approximate level of free convection (LFC) is shown. The mixing line satisfies the instability criterion (25) for unstable unsaturated downdrafts caused by cloud evaporative mixing. Sounding from Zipser and Golden (1979).

so far been developed only with idealized examples. In this section some actual soundings will be presented to illustrate and develop the concept further, primarily in the direction of explaining convective equilibrium structure.

a. Stratocumulus sounding

Randall (1980), Deardorff (1980) and Moeng and Arakawa (1980) have discussed stratocumulus instability at length and confirmed (16), which is simply a reformulation of their criterion. Fig. 13 presents as example a sounding through a stratocumulus layer (Schubert, personal communication, 1981). The mixing curve is shown as heavy dashes between cloud base and the SP of 895 mb air above the inversion. The θ_{vc} isopleth through cloud-base SP is shown dotted. Inequality (16) is not satisfied, as expected for the maintenance of a stratocumulus layer. Surprisingly, perhaps, the lapse rate in the cloud layer is slightly to the right of the moist adiabat, and lies on the mixing line. One aircraft sounding cannot be considered representative, although Schubert *et al.* (1979) present a similar example for a few days later. In Section 6d, we present an average tradewind sounding which is more representative, and which also shows coincidence of the temperature sounding and the mixing line (as does Fig. 2 and some land convective averages not included in this paper). This suggests further study.

b. Colorado tornado sounding (Zipser and Golden, 1979)

Fig. 14 is the 1800 Z sounding from Limon (LIC) on 14 August 1977, from Zipser and Golden (1979), which illustrates the severe storm environment mixing case (Section 5b). The cloud-base SP (and a corresponding wet-bulb θ of 23.5°C) is based on surface observations at 2200 Z, the time of the observed tornadoes. The mixing line shown is drawn between cloud-base *SP* and the environmental *SP* for 600 mb, characteristic of the upper, nearly dry adiabatic layer from 580 to 700 mb, which has a potential temperature of ~45.5°C. Table 3 gives values for the two Saturation Points shown. The θ_{vu} isopleth through the upper SP is drawn (short dashed).

Because cloud-base air has a θ_{vu} below this θ_v isopleth, unsaturated mixtures of cloud and clear air will be negatively buoyant and sink freely in downdrafts in the upper dry layer: that is, inequality (17) is satisfied.

Although cloud-base air is ~3 K colder than the environment (318 K at cloud-base), because of the θ_v correction, its negative buoyancy at cloud-base is only ~1.5°K. In this case where the upper layer is nearly well mixed, the level of free convection is given to sufficient accuracy by the level of intersection of the moist adiabat and the dotted θ_v isopleth. (See Fig. 8 for the exact construction).

TABLE 3. Parameters for tornado sounding SP's.

p	p_{SL}	T_{SL}	θ_{SL}	q_{SL}	θ_{ESL}	θ_{vu}
Cloud-base	685	9.5	315.0	11.0	349.0	317.1
600 mb	485	−14.0	318.8	2.67	327.6	319.3

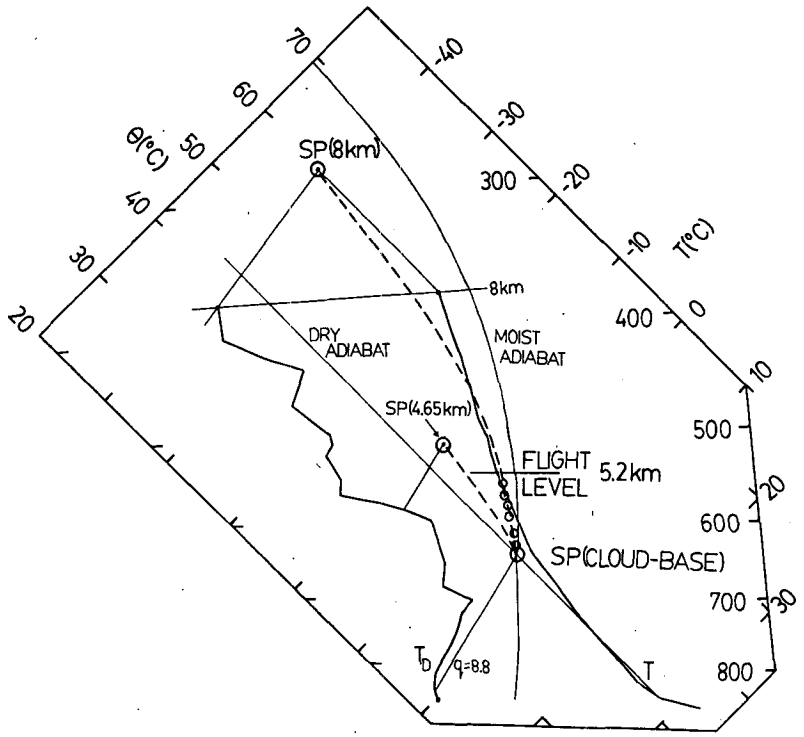

FIG. 15. 1730 Z sounding at Potter on 25 July 1976, showing temperature and dewpoint; two mixing lines between *SP*'s for cloud-base air and air from 8 and 4.65 km. SP's for in-cloud observations are shown (open circles). Sounding from Paluch (1979).

c. *Cloud-top mixing (Paluch, 1979)*

Paluch (1979) showed that in-cloud parameters measured by a sailplane corresponded typically to mixtures between cloud-base air and air from several kilometers above the flight observation level, suggesting mixing down of environmental air entrained through cloud-top. She used mixing diagrams for the conserved parameters: total water and a wet equivalent potential temperature (conserved along a reversible wet adiabat). Fig. 15 is a replot of her Fig. 4 on a tephigram. The SP's of some measurements of in-cloud properties are plotted as small circles: they lie on the mixing line between air from 8 km (SP at 282 mb) and 1.5 km (just above the surface, with SP at the observed cloud-base of 3.8 km, 645 mb). The flight level of the in-cloud observations was 5.2 km. Fig. 15 only shows SP's below the flight level because the sailplane did not measure moisture content in unsaturated air. The mixing line is also drawn between cloud-base air and air from 4.65 km, corresponding approximately to "lateral entrainment" of air into the cloud between cloud-base and the observation level. As Paluch (1979) concluded, it is clear that this mixing process does not characterize the measured in-cloud properties.

θ_v isopleths have not been plotted on this large-scale tephigram for clarity. However, it can be seen qualitatively that just saturated mixtures are negatively buoyant at upper levels, but are near neutral buoyancy (slightly more positive with the θ_v correction) between 460 and 545 mb (the flight observation level), indicating (Paluch, 1979) that air descended in mixtures that are close to buoyancy equilibrium (Telford, 1975).

d. *Trade cumulus equilibrium structure*

The trade cumulus layer involves the mixing of a moist boundary layer with overlying drier, potentially warmer air above the trade inversion. The comparison with the stratocumulus layer is instructive. Fig. 16 presents the average of three days' soundings during BOMEX, a trade-wind experiment, during an undisturbed period. (T, T_D) for the mean sounding are plotted as heavy lines, the open circles are SP's for selected levels (found by the intersection of the dry adiabat through the SP with the T sounding), and the dashed line is the mixing line between cloud-base air and the subsiding air just above the trade inversion.

Several facts are readily apparent:

1) The instability criterion for the breakup of a stratocumulus layer is easily satisfied: θ_E of the subsiding dry air at inversion top is well to the left of

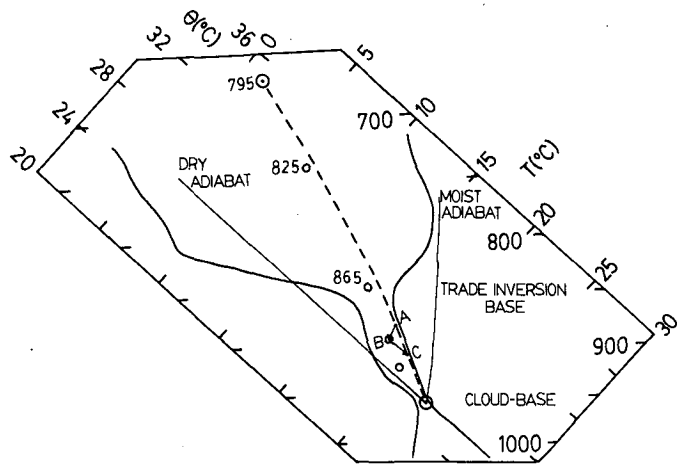

FIG. 16. Three-day average sounding for undisturbed trade-wind convection (BOMEX 22–24 June 1969, data kindly supplied by E. M. Rasmusson). Dashed curve is mixing line between inversion top and subcloud air SP's. Open circles are SP's of environment. Arrow AB denotes generation of environmental SP by radiational cooling of air from mixing line.

both the moist adiabat through cloud-base, and the θ_{vc} isopleth through cloud-base (not shown). The cumulus layer lapse-rate is also well to the left of the moist adiabat.

2) Above the base of the trade inversion, just-saturated mixtures are very cold and will readily sink in downdrafts to near the base of the inversion (Betts, 1973).

3) The lapse-rate in the conditionally unstable cumulus layer, between cloud-base and inversion base, parallels remarkably closely the mixing curve, which does not favor downdrafts in this layer.

4) Within the cumulus layer and trade inversion layer, saturation points of the environment lie to the left of the mixing line.

Since this is an average of some 180 soundings during a 3-day period (22–24 June 1969) of shallow trade-wind convection, it can be regarded as representative (individual day averages show the same features).

Because of 1) and 2) above, overshooting cumulus towers become cooler as they mix in the inversion layer and can readily sink back towards the base of the trade inversion. In this process the SP of a mixture moves up the dashed line from cloud-base. However, unlike a stratocumulus layer where the cloud layer has a nearly wet adiabatic structure, the cumulus layer has a marked θ_{ES} minimum at the trade inversion base. Downdrafts cannot penetrate this level. Indeed, Fig. 16 shows that *no* mixtures of cloud-base and inversion top air are significantly cooler than the environmental profile below the inversion base (the θ_v correction eliminates the small negative temperature difference in Fig. 16). Thus downdrafts are favored above the inversion base, but not below. Betts (1973, 1978) and Cho (1977) have both shown that cloud-induced downward motion dominates above the trade inversion base, but the net cloud-mass flux is upward in the lower cumulus layer.

We conclude that the evaporative mixing, cooling and sinking of overshooting cumulus towers lowers the inversion base θ, and with it steepens the lapse-rate of the lower cumulus layer *until* the latter reaches the dashed mixing curve when further cooling by mixing is not possible.

This explains 3) but not 4): why, that is, the lower cumulus layer is not brought to saturation on the mixing line, but instead has a nearly constant 80% relative humidity (a value of $\mathcal{P} \sim -20$ mb). Further lateral mixing between cloud and this environment, for example, would give cooler mixtures and the layer would tend to saturation at the environment SP's. 4) is certainly an equilibrium state, but it cannot be explained by mixing alone between the two source regions of air: the subcloud layer and inversion top (since all such mixtures would have SP's on the dashed line).

We conclude that radiative cooling of the environment is probably responsible for the deviation of environmental SP's in the cumulus layer from the dashed line. The arrows linking ABC in Fig. 16 show this process: the cooling of just saturated mixtures at constant q (see Fig. 3) to give an environmental SP (A to B) while the parcel sinks to θ_v equilibrium (B to C). The cooling necessary in the middle of the cumulus layer is ~ -1.4°C and at cloud-base less (~ -0.5°C). Cox (1973) calculates a radiative cooling rate of -2°C day^{-1} for the 100 mb layer 967–867 mb, giving a time scale for the radiative cooling

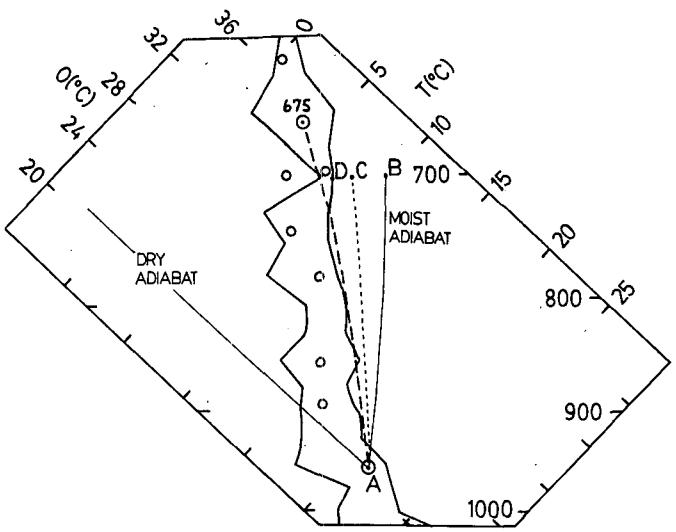

FIG. 17. Sounding for GATE ship *Dallas*, for 1214 Z, Julian Day 257, 1974. T, T_D soundings shown as heavy lines, environmental SP's as open circles. The mixing line between cloud-base SP and environmental air at 675 mb is shown (heavy dashes), and the θ_{vc} isopleth through cloud base (short dashes).

of the environmental SP's ranging from 1.4 to 4 day^{-1}. For comparison, Cho (1977) gives a recycling rate of environmental air by cumulus clouds for the BOMEX data which varies sharply with height from 1.2 day^{-1} at 900 mb to 2.8 day^{-1} at cloud-base. Another rough estimate of this layer recycling rate (using Cho's data) is

$$\frac{\text{cloud mass flux}}{\text{layer depth}} \approx \frac{160 \text{ mb day}^{-1}}{100 \text{ mb}} \approx 1.6 \text{ day}^{-1}.$$

Using Betts' (1975) value of 200 mb day^{-1} for the cloud-base mass flux gives a slightly higher value. The agreement with the radiative timescale estimate is satisfactory (particularly since the BOMEX humidity data needed significant correction).

The intriguing implication of this preliminary analysis is that while the thermal structure of the trade cumulus layer is maintained by a cloud-scale process (the cold downdrafts produced by overshooting cumulus towers), the relative humidity of the layer appears to involve in addition a radiative timescale. This clearly needs further study.

e. GATE convective band inflow sounding

Fig. 17 shows the sounding at 1214 Z on Julian Day 257 from the ship *Dallas* doing the GATE experiment. It is representative of air flowing into a convective band (Zipser *et al.*, 1981). The sounding is quite stable and moist. The open circles show environmental air SP's: the lowest circle (marked A) is the SP of air from near the surface, representative of cloud-base air. The mixing line (heavy dashes) is drawn between A and the SP of 675 mb environmental air, representative of the more stable layer from 650–750 mb, which may be the top of a cumulus layer. This is the mixing line with near-neutral buoyancy. Mixing lines with air from above this level are positively buoyant, indicating that even with continuous mixing with air with cloud-base SP, descent in negatively buoyant downdrafts is not possible. Mixing between cloud-base air and air below 700 mb gives negatively buoyant mixtures, which can descend some way in downdrafts (Sections 3b, 5c). With continuous mixing with cloud air from cloud-base, parcels could descend from 725 mb through the cloud (Telford, 1975).

Fig. 17 also shows (short dashes) the θ_{vc} isopleth for cloudy air through the cloud-base SP to 700 mb (A30). Its meaning is that cloudy air ascending moist adiabatically to point B at 700 mb, without fallout of liquid water, has a buoyancy equivalent to a saturated parcel at point C with no liquid water (see Fig. 8). It is clear that the liquid water loading has greatly reduced cloud parcel buoyancy at 700 mb, where the sounding is nearly saturated (on CD, $\delta\theta \propto \delta\theta_v$, A23). Indeed, if the sounding were saturated, the area between the θ_{vc} isopleth and the sounding curve is related to the available potential energy (See Section 4c). This is qualitatively true for the moist sounding shown, and we can see that the CAPE is dramatically reduced by the water loading. Zipser and Lemone (1980) have commented on the weakness of observed GATE updrafts in relation to the convective available potential energy (as conventionally computed ignoring the negative contribution of liquid water to the buoyancy). One-dimensional models readily show the dynamic significance of the

water loading for GATE clouds (E. J. Zipser, personal communication, 1980). Fig. 17 graphically indicates how buoyancy is markedly reduced until microphysical processes convert and precipitate cloud water.

The next example shows this reduction in buoyancy even more dramatically.

f. Deep convective equilibrium structure

A number of GATE soundings in highly disturbed convective episodes show nearly saturated soundings with lapse-rates through a deep layer that are between dry and moist adiabats and are, therefore, apparently highly unstable. (This was pointed out by Ed Zipser to the author, who had noticed similar soundings for VIMHEX data.) Fig. 18 shows an example: 1213 Z on Julian Day 248 (1974) from the ship *Dallas*. The sounding (during a major disturbance) is nearly saturated from 1000–650 mb and the moist adiabat through the low-level SP (cloud-base) suggests a large convective available potential energy. However, the θ_{vc} isopleth through the cloud-base SP at 990–625 mb (the sounding θ_{ES} minimum) shows that without fallout of cloud water, updrafts are almost neutrally buoyant. This is again consistent with the weak drafts observed in GATE (Zipser and Lemone, 1980). Furthermore, it suggests that in major disturbances, the atmosphere approaches an equilibrium structure that is near neutral to the convective process. Above 625 mb, θ_{ES} for the environment again increases: this is consistent with the fact that above this level precipitation and freezing (freezing level is ~575 mb) significantly increase parcel buoyancy.

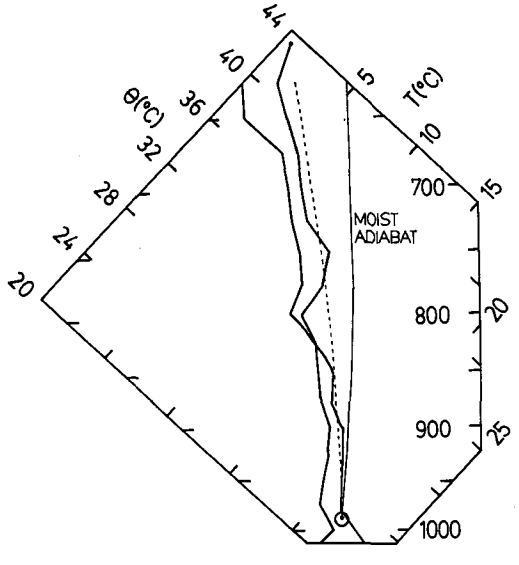

FIG. 18. Sounding for GATE ship *Dallas*, for 1213 Z, Julian Day 248, 1974. The θ_{vc} isopleth (short dashes) and moist adiabat are drawn through a low-level *SP* (at 990 mb).

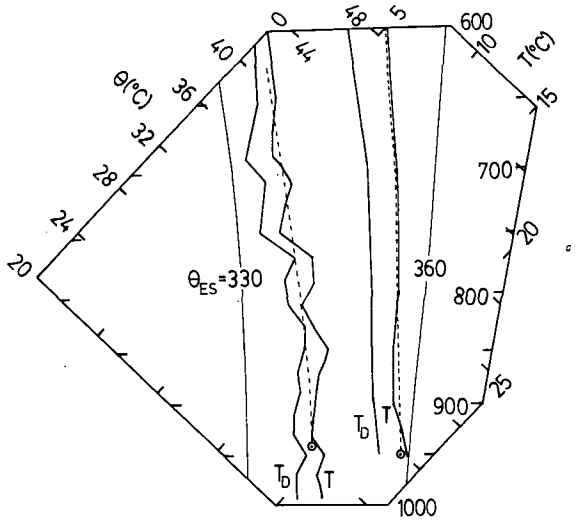

FIG. 19. (T, T_D) sounding for VIMHEX-1972 (No. 317, 1005 LST on 2 September 1972 (curves on left) and composite hurricane sounding (on right) at r = 0.7°, from Frank (1977). Dashed lines indicate slope of θ_{vc} isopleth through a low-level SP.

Fig. 19 shows two other examples, a sounding near the end of a major convective episode during the VIMHEX-1972 experiment, and an average hurricane sounding from Frank (1977), characteristic of the intense convection just beyond the eyewall cloud. Both show the same structure as Fig. 18: a temperature sounding that closely parallels the θ_{vc} isopleth. The mixing curve between the mid-troposphere and the low-level SP is not shown, but clearly it too closely parallels the sounding. Thus, the atmosphere has become near neutral both to mixing and buoyant processes. Parcels can rise buoyantly if liquid water is precipitated, but also sink with negative buoyancy if rain falls into the nearly saturated environment, simply due to the liquid water loading.

The following tentative conclusions can be drawn:

1) The apparently highly unstable soundings in regions of major disturbances are in fact near-neutral in the lower troposphere, until cloud water is converted and precipitated. In other words, the atmosphere appears to establish a convective equilibrium structure in which the mixing curve, and the saturated sounding profile, both approach the θ_{vc} isopleth.

2) The θ_{vc} isopleth for cloudy air is of great significance. It indicates that the reference process for the buoyancy on ascent of a cloud parcel is only $0.9\Gamma_W$ (A30) until the cloud water is converted and precipitated.

This is clearly of significance to simple cloud modeling, lapse-rate adjustment models for convective parameterization, and the establishment of a quasi-equilibrium structure (Manabe *et al.*, 1965; Betts, 1973; Arakawa and Schubert, 1974). In closing, it is noted that the three examples in Figs. 18, 19 char-

acterize major rain episodes, but do not have the large low-level decreases of θ_E caused by strong unsaturated downdrafts, as occur in traveling squall systems (Zipser, 1977; Miller and Betts, 1977).

7. Closing remarks

This paper has covered considerable ground in a largely conceptual and illustrative manner. The main conclusions are summarized here.

1) The use of the Saturation Point (SP) consolidates and simplifies the description of the moist thermodynamics of cloudy air. It compactly represents the conserved parameters and suggests a coordinate system for simple cloud models. (This work will be continued in another paper.) It simplifies the representation of clear and cloudy air (but not precipitation) on a thermodynamic diagram (the tephigram was used in this paper).

2) The use of the SP enables the simple representation of the mixing process between air parcels (whether clear or cloudy) originating from any level in the atmosphere, in terms of a mixing line on a thermodynamic diagram. The relationship of the mixing line to the atmospheric stratification is made readily visible, and questions such as the minimum temperature from an evaporative mixing process are easily answered.

3) The use of the SP permits the representation of virtual potential temperature isopleths on a thermodynamic diagram for both unsaturated and cloudy domains. This is a significant advance in the use of the thermodynamic diagram, since questions of parcel buoyancy, available potential energy, parcel equilibrium level, level of free convection (with θ_v correction) become readily visible.

4) Taken together, 2) and 3) allow the diagrammatic representation of instabilities due to evaporative mixing. As well as expressing the well-known cloud-top entrainment instability for a stratocumulus layer in these terms, we have also shown that an analogous but contrasting downdraft instability exists in the severe storm atmosphere. For the stratocumulus layer, the mixing of some dry air from the inversion into the cloud layer produces unstable cloudy downdrafts in the moist adiabatic cloud layer, provided θ_E of the entrained clear air is low enough. For the severe storm environment the mixing of some cloud air out into a nearly dry adiabatic upper mixed layer produces unstable, unsaturated downdrafts provided the cloud θ_L is low enough. These two extremes were contrasted with the production of downdrafts by mixing in a cumulus layer which has a more intermediate structure. In the cumulus layer, cool downdraft production requires that the slope of the mixing line be to the left of the sounding temperature profile (i.e., cooler), but even so, mixtures can only descend part way to cloud base.

5) The use of the mixing line and the θ_v isopleths suggests explanations for the equilibrium structure of the convective atmosphere. A specific illustration shows the equilibrium thermal structure of the lower trade cumulus layer lies on the mixing line between air from the subcloud layer and from the inversion top. It is suggested that radiative cooling may be responsible for the deviation of the SP's in the cloud layer from the mixing line.

Other examples for the highly disturbed tropical atmosphere over the ocean (GATE) over land (VIMHEX) and an inner hurricane rain area composite (Frank, 1977) show that the apparently conditionally unstable thermal structure in the lower troposphere parallels the θ_{vc} isopleth (for air ascending with cloud water). This suggests that rather than being unstable, the atmosphere has approached a near-neutral condition for the process.

6) The mixing line representation supports the inference of cloud-top mixing in Colorado cumulus clouds from soundings and aircraft observations (Paluch, 1979), and the θ_v representation permits buoyancy comparisons to be made.

7) The θ_{vc} isopleth shows that the buoyancy reference process for cloudy air is only 0.9 of the moist adiabatic lapse-rate (until liquid water is precipitated). This markedly reduces convective available potential energy and suggests an explanation for the low updraft velocities in GATE cumulonimbus clouds.

Clearly many of these topics require further exploration using other atmospheric data sets. The principle advantage of the tephigram approach used here is that soundings are routinely plotted on thermodynamic diagrams. The addition of the SP's, some sample mixing lines and the θ_v isopleths (on moveable overlays) gives a wealth of new insights into convective structure and processes; instabilities and equilibrium, downdraft and updraft properties. These diagrams facilitate comparison of different convective atmospheres and the transitions between them, and for many purposes are sufficiently accurate (given the errors in real sounding data).

Acknowledgments. This work was supported by the Atmospheric Science Division (GARP program) of the National Science Foundation under grant ATM-7915788. The idea for the work originated while the author was a visiting scientist at NCAR (which is also funded by the National Science Foundation).

I am grateful to E. J. Zipser for this additional research support, and for valuable discussions. I also acknowledge discussions and data from I. R. Paluch, W. H. Schubert, B. A. Albrecht, E. M. Rasmusson and J. H. Golden. I thank reviewers and the faculty and students at SUNY (Albany) for clarifying parts of the text.

APPENDIX

Thermodynamic Parameters

a. *Symbol convention*

Devising a simple notation for the multitude of symbols in Fig. 1 is not easy, particularly since many are in conventional use. A subscript notation will be used here in which subscript W denotes a variable defined on the moist adiabat through the SP, L a variable defined on the dry adiabat (constant θ_L), and D on the constant q line (dewpoint line). Table 4 summarizes the meaning of these symbols. For example, if a parcel descends through its saturation level and hence changes from being cloudy to unsaturated, the interpretation of θ_L changes as θ_L reduces to θ, while that of θ_{EL} changes from $\theta_{ES}(T_L, p)$ to $\theta_{ES}(T, p)$ etc. The value of having the general symbolic notation is that the thermodynamic relationships discussed in the next section become independent of whether a parcel is cloudy or unsaturated. The general symbols for the conserved variables are placed in parentheses in Table 4, because whatever the parcel pressure p, these always have their saturation level values, which we have given special symbols, subscripted SL (Section 2b). For example,

$$\theta_L(p) = \theta(p_{SL}) = \theta_{SL}\,,$$

$$\theta_{EW}(p) = \theta_{ES}(p_{SL}) = \theta_{ESL}\,.$$

TABLE 4. Symbol convention.

Parameter specified at parcel pressure p			Parameter specified at p_{SL}
Unsaturated air	Cloudy air	General symbol	Conserved parameters
θ	θ_L	(θ_L)	θ_{SL}
θ_W	θ	θ_W	
θ_D	θ_{DT}	θ_D	
$\theta_{ES}(T)$	$\theta_{ES}(T_L)$	θ_{EL}	
θ_E	$\theta_{ES}(T)$	(θ_{EW})	θ_{ESL}
$\theta_{ES}(T_D)$	$\theta_{ES}(T_{DT})$	θ_{ED}	
$q_s(T)$	q_L	q_L	
q_W	$q_s(T)$	q_W	
q	$q_T = q_S + l$	(q_D)	q_{SL}

b. *Linear relationships (Fig. 1)*

There are six useful linearizations of the gradients of the θ, θ_{ES}, q_S lines on a thermodynamic diagram (Fig. 1). These can be written with the symbol convention of Table 4:

$$\theta_{SL} - \theta_W(p) = \left(\frac{\partial\theta}{\partial p}\right)_{\theta_{ES}} \mathcal{P}, \qquad \text{(A1)}$$

$$\theta_{SL} - \theta_D(p) = \left(\frac{\partial\theta}{\partial p}\right)_{q_S} \mathcal{P}, \qquad \text{(A2)}$$

$$\theta_{ESL} - \theta_{EL}(p) = \left(\frac{\partial\theta_{ES}}{\partial p}\right)_{\theta} \mathcal{P}, \qquad \text{(A3)}$$

$$\theta_{ESL} - \theta_{ED}(p) = \left(\frac{\partial\theta_{ES}}{\partial p}\right)_{q_S} \mathcal{P}, \qquad \text{(A4)}$$

$$q_{SL} - q_W(p) = \left(\frac{\partial q_S}{\partial p}\right)_{\theta_{ES}} \mathcal{P}, \qquad \text{(A5)}$$

$$q_{SL} - q_L(p) = \left(\frac{\partial q_S}{\partial p}\right)_{\theta} \mathcal{P}, \qquad \text{(A6)}$$

where

$$\left(\frac{\partial\theta}{\partial p}\right)_{\theta_{ES}} \equiv \left(\frac{\partial\theta_{SL}}{\partial p_{SL}}\right)_{\theta_{ESL}}$$

is simply the change of θ with pressure along a moist adiabat in Fig. 1, etc. For example, for cloudy air ($\mathcal{P} > 0$), (A5) becomes (Table 4) the well-known

$$l = \left(\frac{\partial q_S}{\partial p}\right)_{\theta_{ES}} \mathcal{P}, \qquad \text{(A5')}$$

while for unsaturated air ($\mathcal{P} < 0$), (A6) would give the subsaturation

$$q_S - q = -\left(\frac{\partial q_S}{\partial p}\right)_{\theta} \mathcal{P}. \qquad \text{(A6')}$$

The gradients in (A1) to (A6) are further interrelated through the definition of θ_{ES}

$$C_p \frac{\delta\theta_{ES}}{\theta_{ES}} = C_p \frac{\delta\theta}{\theta} + L\frac{\delta q_S}{T}\,. \qquad \text{(A7, 1b)}$$

This involves slight approximation if L, C_p are taken constant. It follows from (A7) that

$$\Gamma_W = \left(\frac{\partial\theta}{\partial p}\right)_{\theta_{ES}} = -\frac{L\bar{\theta}}{C_p\bar{T}}\left(\frac{\partial q_S}{\partial p}\right)_{\theta_{ES}}, \qquad \text{(A8)}$$

$$\left(\frac{\partial\theta_{ES}}{\partial p}\right)_{\theta} = \frac{L\bar{\theta}_{ES}}{C_p\bar{T}}\left(\frac{\partial q_S}{\partial p}\right)_{\theta}, \qquad \text{(A9)}$$

$$\left(\frac{\partial\theta}{\partial p}\right)_{q_S} = \frac{\bar{\theta}}{\bar{\theta}_{ES}}\left(\frac{\partial\theta_{ES}}{\partial p}\right)_{q_S}, \qquad \text{(A10)}$$

where mean values of T, θ, θ_{ES}, have been inserted. These are simply relationships between the parameters from which the tephigram is constructed. They are equally valid written in terms of θ_{SL}, q_{SL}, θ_{ESL}, p_{SL}. (A8) is well-known and when substituted in (A1), (A5) gives

$$C_p[\theta_{SL} - \theta_W(p)] = \frac{L\bar{\theta}}{\bar{T}}[q_W(p) - q_{SL}], \qquad \text{(A11)}$$

which for unsaturated air simplifies to the definition of the wet-bulb temperature

$$C_p(T - T_W) = L(q_W - q), \qquad \text{(A12)}$$

while for cloudy air (A11) gives the approximation for θ_L

$$C_p(\theta_L - \theta) = -\frac{L\bar{\theta}}{\bar{T}} l. \qquad \text{(A12')}$$

(A9) substituted in (A3) and (A6) gives

$$\theta_{EL}(p) - \theta_{ESL} = \frac{L\bar{\theta}_{ES}}{C_p\bar{T}}(q_L(p) - q_{SL}), \qquad \text{(A13)}$$

which reduces for $\mathcal{P} < 0$ to

$$\theta_{ES}(p) - \theta_E = \frac{L\bar{\theta}_{ES}}{C_p\bar{T}}(q_S - q), \qquad \text{(A14)}$$

which relates $\theta_{ES} - \theta_E$ for unsaturated air to its subsaturation, and is fairly well-known, e.g., Betts (1974). Similarly, (A10) substituted in (A2) and (A4) gives

$$\theta_{SL} - \theta_D(p) = \frac{\bar{\theta}}{\bar{\theta}_{ES}}[\theta_{ESL} - \theta_{ED}(p)], \qquad \text{(A15)}$$

which reduces for $\mathcal{P} < 0$ to

$$\theta - \theta_D = \frac{\bar{\theta}}{\bar{\theta}_{ES}}[\theta_E - \theta_{ES}(T_D)]. \qquad \text{(A16)}$$

This relates the dewpoint θ depression to the θ_E depression of the dewpoint temperature, and together with (A10), (A4) has (to the author's knowledge) not yet found a use.

We include all these relationships for completeness, since they are all implied in Fig. 1, together with the Clausius-Clapyron relationship, which is approximately (isobarically)

$$\left(\frac{\partial q_S}{\partial T}\right)_p \approx \frac{Lq_S}{R_V T^2} = \frac{\alpha}{T}, \qquad \text{(A17)}$$

where $\alpha = Lq_S/R_V T$, and R_V is the gas constant for water vapor. This can be used to relate isobaric changes of θ, θ_{ES} (Betts, 1973) by substituting in (A7)

$$\frac{\delta\theta_{ES}}{\theta_{ES}} \approx (1 + \gamma)\frac{\delta\theta}{\theta}, \qquad \text{(A18)}$$

where we define the symbols (see also Section 4b)

$$\gamma = \frac{L^2 q_S}{C_p R_V T^2} = \left(\frac{Lq_S}{R_V T}\right)\left(\frac{L}{C_p T}\right) = \frac{\alpha}{\epsilon},$$

where $\epsilon = C_p T/L$. Thus, in gradient form, we may write for an arbitrary $\partial\theta/\partial p$ (Betts, 1973)

$$\frac{\bar{\theta}}{\bar{\theta}_{ES}}\left(\frac{\partial\theta_{ES}}{\partial p}\right) = (1 + \gamma)\left[\frac{\partial\theta}{\partial p} - \left(\frac{\partial\theta}{\partial p}\right)_{\theta_{ES}}\right]. \qquad \text{(A19)}$$

For the dry adiabat, $\partial\theta/\partial p = 0$ and A19 becomes

$$\frac{\bar{\theta}}{\theta_{ES}}\left(\frac{\partial\theta_{ES}}{\partial p}\right)_\theta = -(1 + \gamma)\Gamma_W, \qquad \text{(A20)}$$

defining Γ_W as in (A8). This relates the gradient of θ_{ES} on the dry adiabat to the gradient of θ on the moist adiabat.

c. *Gradient of θ_v isopleths*

1. Unsaturated region: $\mathcal{P} < 0$

Consider the triangle ADE in Fig. 7: the gradients are related by

$$0 = \left(\frac{\partial\theta_{SL}}{\partial p_{SL}}\right)_{\theta_{vu}} + \left(\frac{\partial\theta_{SL}}{\partial\theta_{vu}}\right)_{pSL}\left(\frac{\partial\theta_{vu}}{\partial p_{SL}}\right)_{\theta_{SL}}. \qquad \text{(A21)}$$

At constant p_{SL} from (13a')

$$\frac{\delta\theta_{vu}}{\bar{\theta}_{vu}} = \frac{\delta\theta_{SL}}{\bar{\theta}_{SL}} + \frac{0.61\delta q_{SL}}{1 + 0.61\bar{q}_{SL}}. \qquad \text{(A22)}$$

Substituting the Clausius-Clapyron equation from (A17) in the form

$$\delta q_{SL} = \alpha\delta\theta_{SL}/\bar{\theta}_{SL},$$

gives

$$\left(\frac{\partial\theta_{SL}}{\partial\theta_{vu}}\right)_{pSL} = \frac{1}{1 + 0.61\alpha'}, \qquad \text{(A23)}$$

where

$$\alpha' = \left(\frac{L}{R_V T} + 1\right)q_S.$$

Now

$$\left(\frac{\partial\theta_{vu}}{\partial p_{SL}}\right)_{\theta_{SL}} = 0.61\left(\frac{\partial q_{SL}}{\partial p_{SL}}\right)_{\theta_{SL}} = 0.61\epsilon(1 + \gamma)\Gamma_W, \qquad \text{(A24)}$$

substituting (A9), (A20) (which are equally valid in terms of p_{SL}, θ_{SL}, etc.). Substituting (A23), (A24) in (A21) gives

$$\left(\frac{\partial\theta_{SL}}{\partial p_{SL}}\right)_{\theta_{vu}} = \frac{0.61(\epsilon + \alpha)}{1 + 0.61\alpha'}\Gamma_W = \beta_1\Gamma_W, \qquad \text{(A25)}$$

since $\alpha = \gamma\epsilon$. Table 2 shows that β_1 increases with q_S.

2. Cloudy region: $\mathcal{P} > 0$

A similar analysis for the saturated cloudy region shows that the θ_{vc} isopleths deviate from the moist adiabat in Fig. 7 by a small (nearly constant) fraction of its slope. Considering the triangle ABC in Fig. 7, the gradients are related by

$$\left(\frac{\partial\theta_{SL}}{\partial p_{SL}}\right)_{\theta_{ES},p} = \left(\frac{\partial\theta_{SL}}{\partial p_{SL}}\right)_{\theta_{vc},p} + \left(\frac{\partial\theta_{SL}}{\partial\theta_{vc}}\right)_{pSL,p}\left(\frac{\partial\theta_{vc}}{\partial_{pSL}}\right)_{\theta_{ES},p}. \qquad \text{(A26)}$$

The left-hand side is just Γ_W. At constant p, p_{SL} from (13b')

$$\frac{\delta\theta_{vc}}{\bar{\theta}_{vc}} = \frac{\delta\theta}{\bar{\theta}} + \frac{0.61\delta q_S}{1 + 0.61q_S - l} - \frac{\delta l}{1 + 0.61q_S - l}.$$

Neglecting the small terms in l, δl, we obtain the equivalent of (A23):

$$\left(\frac{\partial\theta_{SL}}{\partial\theta_{vc}}\right)_{p_{SL},p} \simeq \frac{1}{1 + 0.61\alpha'}. \qquad \text{(A27)}$$

Finally,

$$\left(\frac{\partial\theta_{vc}}{\partial p_{SL}}\right)_{\theta_{ES},p} = -\theta\left(\frac{\partial l}{\partial p_{SL}}\right)_{\theta_{ES},p}, \qquad \text{(A28)}$$

since θ, q_S do not change if θ_{ES}, p are kept constant. Therefore,

$$\left(\frac{\partial\theta_{vc}}{\partial p_{SL}}\right)_{\theta_{ES},p} = \theta\left(\frac{\partial q_{SL}}{\partial p_{SL}}\right)_{\theta_{ES},p} = \epsilon\Gamma_W, \qquad \text{(A29)}$$

substituting from (A8). Substituting (A27), (A29) in (A26) gives

$$\Gamma_W - \left(\frac{\partial\theta_{SL}}{\partial p_{SL}}\right)_{\theta_{vc},p} = \left(\frac{\epsilon}{1 + 0.61\alpha'}\right)\Gamma_W = \beta_2\Gamma_W. \qquad \text{(A30)}$$

Table 2 shows that $\beta_2 \approx 0.1$ for all q_S.

REFERENCES

Arakawa, A., and W. Schubert, 1974: Interaction of a cumulus cloud ensemble with the large-scale environment: Part I. *J. Atmos. Sci.*, **31**, 674–701.

Albrecht, B. A., A. K. Betts, W. H. Schubert and S. K. Cox, 1979: A model of the thermodynamic structure of the trade-wind boundary layer: Part I. Theoretical formulation and sensitivity tests. *J. Atmos. Sci.*, **36**, 73–89.

Betts, A. K., 1973: Non-precipitating convection and its parameterization. *Quart. J. Roy. Meteor. Soc.*, **99**, 178–196.

——, 1975: Parametric interpretation of trade-wind cumulus budget studies. *J. Atmos. Sci.*, **32**, 1934–1945.

——, 1978: Convection in the tropics. *Meteorology over the Tropical Oceans, Quart. J. Roy. Meteor. Soc.* Suppl., 105–132.

——, and M. F. Silva Dias, 1979: Unsaturated downdraft thermodynamics in cumulonimbus. *J. Atmos. Sci.*, **36**, 1061–1071.

Bolton, D., 1980: The computation of equivalent potential temperature. *Mon. Wea. Rev.*, **108**, 1046–1053.

Cho, Han-Ru, 1977: Contributions of cumulus cloud life-cycle effects to the large-scale heat and moisture budget equations. *J. Atmos. Sci.*, **34**, 1061–1071.

Cox, S. K., 1973: Radiation components of the energy budget for BOMEX. Atmos. Sci. Pap. No. 208, Colorado State University, 43 pp. [NTIS-COM73-11950].

Deardorff, J. W., 1976: On the entrainment rate of a stratocumulus topped mixed layer. *Quart. J. Roy. Meteor. Soc.*, **102**, 563–582.

——, 1980: Cloud-top entrainment instability. *J. Atmos. Sci.*, **37**, 131–147.

Frank, W. M., 1977: The structure and energetics of the tropical cyclone, I: Storm structure. *Mon. Wea. Rev.*, **105**, 1119–1135.

Fraser, A. B., 1968: The white box: the mean mechanics of the cumulus cycle. *Quart. J. Roy. Meteor. Soc.*, **94**, 71–87.

Fujita, R., and F. Caracena, 1977: An analysis of three weather-related aircraft accidents. *Bull. Amer. Meteor. Soc.*, **58**, 1164–1181.

Kamburova, P. L., and F. H. Ludlam, 1966: Rainfall evaporation in thunderstorm downdrafts. *Quart. J. Roy. Meteor. Soc.*, **92**, 510–518.

Lilly, D. K., 1968: Models of cloud-topped mixed layers under a strong inversion. *Quart. J. Roy. Meteor. Soc.*, **94**, 292–309.

Lord, S. J., and A. Arakawa, 1980: Interaction of a cumulus cloud ensemble with the large-scale environment: Part II. *J. Atmos. Sci.*, **37**, 2677–2692.

Ludlam, F. H., 1966: Cumulus and cumulonimbus convection. *Tellus*, **18**, 687–698.

——, 1980: *Clouds and Storms.* Pennsylvania State University Press, 239–246.

Manabe, S., J. Smagorinsky and R. F. Strickler, 1965: Simulated climatology of a general circulation model with a hydrological cycle. *Mon. Wea. Rev.*, **93**, 769–798.

Miller, M. J., and A. K. Betts, 1977: Traveling convective storms over Venezuela. *Mon. Wea. Rev.*, **105**, 833–848.

Moeng, C-H., and A. Arakawa, 1980: A numerical study of a marine subtropical stratus cloud layer and its stability. *J. Atmos. Sci.*, **37**, 2661–2676.

Moncrieff, M. W., and M. J. Miller, 1976: The dynamics and simulation of tropical cumulonimbus and squall lines. *Quart. J. Roy. Meteor. Soc.*, **102**, 373–394.

Paluch, I. R., 1979: The entrainment mechanism in Colorado cumuli. *J. Atmos. Sci.*, **36**, 2467–2478.

Randall, D. A., 1980: Conditional instability of the first kind upside-down. *J. Atmos. Sci.*, **37**, 125–130.

Rossby, C. G., 1932: Thermodynamics applied to air mass analysis. *Meteor. Pap.*, Vol. 1, Massachusetts Institute of Technology, 7–24.

Saunders, P. M., 1957: The thermodynamics of saturated air: a contribution to the classical theory. *Quart. J. Roy. Meteor. Soc.*, **83**, 342–350.

Schubert, W. H., 1976: Experiments with Lilly's cloud-topped mixed layer model. *J. Atmos. Sci.*, **33**, 436–446.

——, J. S. Wakefield, E. J. Steiner and S. K. Cox, 1979: Marine stratocumulus convection. Part I: Governing equations and horizontally homogeneous solutions. *J. Atmos. Sci.*, **36**, 1286–1307.

Simpson, R. H., 1978: On the computation of equivalent potential temperature. *Mon. Wea. Rev.*, **108**, 124–130.

Telford, J. W., 1975: Turbulence, entrainment and mixing in cloud dynamics. *Pure Appl. Geophys.*, **113**, 1067–1084.

Zipser, E. J., 1977: Mesoscale and cloud-scale downdrafts as distinct components of squall-line structure. *Mon. Wea. Rev.*, **105**, 1568–1589.

——, and M. A. Lemone, 1980: Cumulonimbus vertical velocity events in GATE. Part II: Synthesis and model core structure. *J. Atmos. Sci.*, **37**, 2458–2469.

——, and J. H. Golden, 1979: A summertime tornado outbreak in Colorado: Mesoscale environment and structural features. *Mon. Wea. Rev.*, **107**, 1328–1342.

——, R. J. Meitin and M. A. Lemone, 1981: Mesoscale motion fields in association with a slow moving GATE convective band. *J. Atmos. Sci.*, **38**, 1725–1750.